Neural Circuitry of Retinal Receptive Fields in Primate

Christopher M. Davenport

A dissertation submitted in partial fulfillment of the
requirements for the degree of

Doctor of Philosophy

University of Washington

2007

Program Authorized to Offer Degree:

Neurobiology and Behavior

University of Washington
Graduate School

This is to certify that I have examined this copy of a doctoral dissertation
by

Christopher M. Davenport

and have found that it is complete and satisfactory in all respects,
and that any and all revisions required by the final
examining committee have been made.

Chair of the Supervisory Committee

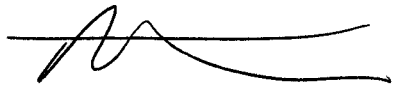

Peter Detwiler

Reading Committee:

Peter Detwiler

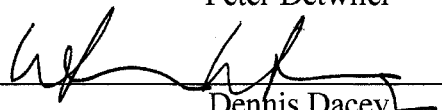

Dennis Dacey

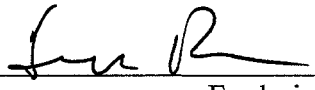

Frederick Rieke

Date: 5/31/2007

In presenting this dissertation in partial fulfillment of the requirements for the doctoral degree at the University of Washington, I agree that the Library shall make its copies freely available for inspection. I further agree that extensive copying of the dissertation is allowable only for scholarly purposes, consistent with "fair use" as prescribed in the U.S. Copyright law. Requests for copying or reproduction of this dissertation may be referred to ProQuest Information and Learning, 300 North Zeeb Road, Ann Arbor, MI 48106-1346, 1-900-521-0600, to whom the author has granted "the right to reproduce and sell (a) copies of the manuscript in microform and/or (b) printed copies of the manuscript made from microform."

Signature 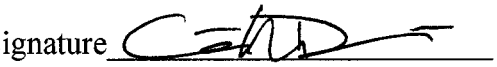

Date 5/31/2007

University of Washington

Abstract

Neural circuitry of retinal receptive fields in primate

Christopher M. Davenport

Chair of the Supervisory Committee:
Professor Peter Detwiler
Physiology and Biophysics Department

The retina contains the first stages of the neural encoding of visual information that begins the generation of our perception of the visual world. The retina contains as many as 70 distinct cell types that interact in specific circuits that process distinct aspects of visual stimuli. The majority of these cell types and circuits are not well understood physiologically and functionally. In this thesis I will describe experiments that examine how specific retinal neurons interact with each other to form their receptive fields and process visual information. In the first chapter I will describe pharmacological and calcium imaging experiments that suggest that A1 axon bearing amacrine cell dendrites are input structures and its axons are output structures. In the second chapter I will test the effect of HEPES and other pH buffers on measures of horizontal cell feedback in primate retina and show results that are consistent with horizontal cell feedback requiring local pH changes in the outer retina. In the third chapter I will present evidence that the blue-yellow opponency in the small bistratified ganglion cell is generated predominantly by horizontal cell feedback, not antagonistic ON and OFF pathway inputs, as previously thought.

TABLE OF CONTENTS

Page

LIST OF FIGURES

LIST OF TABLES

ACKNOWLEDGEMENTS

Getting through nearly six years of graduate school required the help of many people. I would like to thank the following people: Neurobiology and Behavior Graduate Program directors Neil Nathanson, Albert Fuchs, Mike Shadlen and Tom Reh, and office staff members Lucia Wisdom and Ann Wilkinson. The Physiology and Biophysics Department office staff members Marylinne Cunnington, Tina Schulstadt, Liz Fee, Lisa Allen and Jennifer Carillo. Peter Detwiler and Dennis Dacey for their support, discussions, ideas, and teachings both explicit and not. My committee members Fred Rieke, Marc Binder, Les Westrum and Steve Buck. My labmates David Margolis, Andrew Gartland, Greg Newkirk, Patrick Theer and Fred Soo, Orin Packer, Beth Peterson, Toni Haun and Julian Vrieslander. My classmates and fellow graduate students, in particular Zach Scheiner, Doug Wacker, Ken Custer, Sara Custer, Tim Hanks, Jonathan Ting and Marc Morris. My parents, James and Deborah Davenport and my fiancée Lindsay Schwarz.

DEDICATION

To my grandmother, Gloria Morgan, who passed away during my time in graduate school.

Introduction

Our experience of the richness and beauty of the visual world begins with the absorption of photons by specialized photoreceptor cells in the retina at the back of the eye. The resulting photoreceptor signal initiates the neural events that encode image information and form our perception of the world. The vertebrate retina is a layered structure that contains three cell body or nuclear layers interposed with two synaptic or plexiform layers. The cell body layers contain the somata of the five major classes of retinal neurons, photoreceptors, horizontal cells, bipolar cells, amacrine cells and ganglion cells, which interact with each other synaptically in the plexiform layers (Fig 1). The retina is an excellent model for sensory processing, and for neural interactions in general. It can be isolated and kept alive for many hours in vitro. In isolating it, only the output, the optic nerve, is severed so all of the retinal circuitry is kept intact. It can be stimulated by its natural stimulus, light. Finally, it's anatomical structure and pharmacological targets are very well defined. In this introduction I will generally describe the structure and major synaptic interactions that occur in the retina and then specifically describe the cells and pathways relevant to this dissertation. The first section is drawn primarily from a number of excellent books and reviews of retinal anatomy and function (Polyak, 1941; Dowling, 1970; Rodieck, 1988; Dacey, 1994; Rodieck, 1998; Sterling, 1999; Masland, 2001; Sterling, 2004; Wassle, 2004; Callaway, 2005).

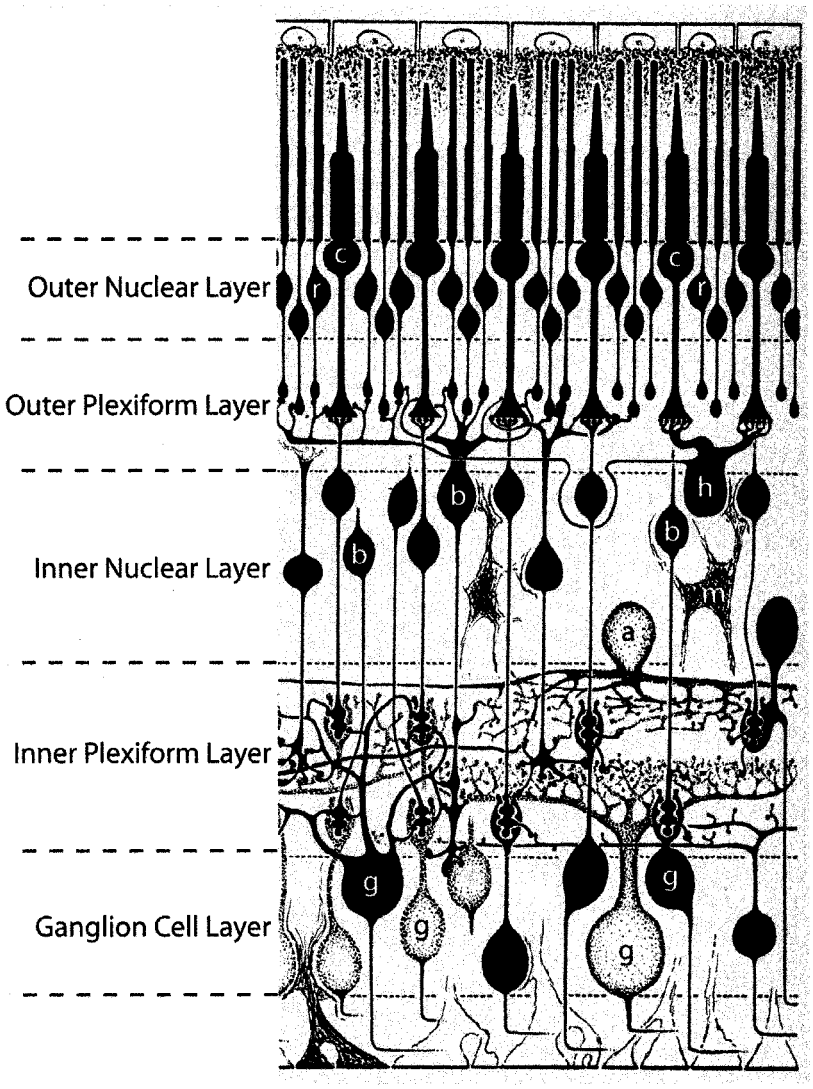

Figure 1: Retinal organization.
The major retinal layers are designated at the left, and the cells within them are labelled as follows c: cone pthotoreceptors; r: rod photoreceptors; b: bipolar cells; h: horizontal cells; a: amacrine cells; g: ganglion cells; m: Müller glia. The diversity of morphology of retinal cells is apparent, especially in bipolar and ganglion cells. Adapted from Polyak, 1941.

Retina Overview

Photoreceptors

Photoreceptors, whose cell bodies occupy the outer nuclear layer (ONL), have elongated outer segments that contain the light absorbing pigment, one of a class of molecules called opsins, and the transduction machinery that converts the absorption of photons in to an electrical signal. They can be broadly divided into two classes, rods and cones, based upon their morphological and physiological properties (Fig 2). Rod photoreceptors have a more cylindrical, thin outer segment and are specialized to mediate vision at very low light levels. Cone photoreceptors have a more conical, tapered outer segment. Cones mediate vision at higher light levels and are responsible for color vision. The results in this dissertation will be based upon cone-mediated responses in retinal neurons.

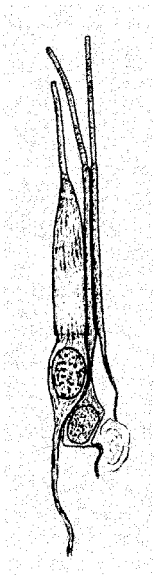

Figure 2: Photoreceptor morphology.
A cone photoreceptor (left) and two rod photoreceptors (right). The rod outer segments are thin and rod-like, the cone outer segment is thicker and tapered. From Polyak, 1941.

Human cones can be divided into long (L), middle (M) and short (S) wavelength sensitive subtypes depending on the wavelength of light to which they are maximally sensitive. Their spectral sensitivity is determined by the specific opsin that they express. L, M and S cones contain opsins which are maximally sensitive to light at ~560, 530 and 430 nm, respectively (Schnapf et al., 1987). Photoreceptor axons extend into the outer plexiform layer (OPL) and form a specialized presynaptic terminal called the pedicle in and around which postsynaptic processes are arrayed.

In darkness, rod and cone photoreceptors contain a high level of cyclic guanosine monophosphate (cGMP) that binds to and opens cyclic nucleotide gated (CNG) channels. These are non-selective cation channels that depolarize the photoreceptor in darkness, causing steady release of the neurotransmitter glutamate (Glu) from their axon terminals. Light activates a G-protein coupled enzyme cascade that stimulates cGMP specific phosphodiesterase and the resulting fall in [cGMP] closes CNG channels and hyperpolarizes the photoreceptor. This decreases the release of Glu and signals an increase in light intensity to postsynaptic neurons (reviewed in Burns and Arshavsky, 2005).

Bipolar Cells

Bipolar cell bodies occupy the inner nuclear layer (INL). They extend dendrites into the OPL and axons into the inner plexiform layer (IPL). They are postsynaptic to photoreceptors and possibly horizontal cells and are presynaptic to ganglion cells and amacrine cells. Bipolar cells can be divided into ~10 subtypes based on morphological properties such as the detailed structure and stratification pattern of their dendrites and

axons in the OPL and IPL, respectively (Fig 3). Glutamate released from photoreceptors has different effects on different populations of bipolar cells depending on the glutamate receptor subtype that is expressed in those bipolar cells. One population, whose dendrites extend deep into the invagination of the cone pedicle express metabotropic glutamate receptor type 6 (mGluR6), which produces a hyperpolarizing response to glutamate (Vardi et al., 2000). These are called ON bipolar cells because they are depolarized by the light-evoked decrease in glutamate release from photoreceptors. ON bipolar cells extend

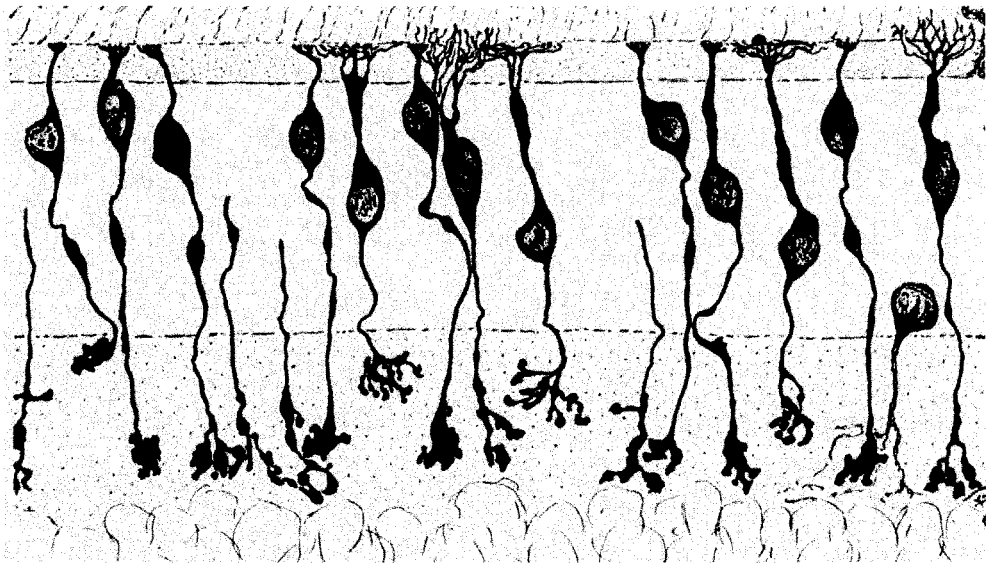

Figure 3: Bipolar cell morphology.
Drawings of Golgi-stained macaque bipolar cells. Note the different dendritic and axonal morphologies, in particular the variable level of stratification of the axon terminals in the IPL. From Polyak, 1941.

axons into the inner portion of the IPL, and their postsynaptic target cells with dendrites in the inner IPL also exhibit ON responses to light. A second major class of bipolar cells have dendrites that terminate at the lateral edge of the cone pedicle invagination and express ionotropic AMPA/Kainate type glutamate receptors that produce depolarizing responses to glutamate (Calkins, 2005). These are called OFF bipolar cells because they

are depolarized by the increase in glutamate release from cones caused by a decrease in light intensity. OFF bipolar cell axons terminate in the outer portion of the IPL, and cells whose dendrites they contact also have OFF light responses. This division of the photoreceptor output into two separate pathways is an example of the multiple parallel neural circuits in the retina that encode separate parts of the visual world by responding differently to light via their connectivity and physiological properties. It is also an example of how morphological differences in retinal cells correlate with physiological differences. In addition to the division of bipolar cell types into ON and OFF classes there are other subtypes that connect to rods, specific cone types, or that display transient or sustained light responses (Wassle and Boycott, 1991; Sterling, 2004).

Horizontal cells

Horizontal cell bodies are located in the INL. They extend dendrites into the OPL that are postsynaptic to photoreceptors and presynaptic to photoreceptors and possibly bipolar cells. Their dendrites serve as both input and output structures. Horizontal cells in the primate retina can be divided into three subtypes based upon their morphology and connectivity to specific photoreceptor types (Fig 4) (Ahnelt and Kolb, 1994b, 1994a; Kolb et al., 1994). HI horizontal cell dendrites contact L and M almost exclusively. The H1 cell has a single axon that travels some distance across the retina before forming an arborization that contacts rod photoreceptors. The dendritic and axonal arbors are electrically isolated by the long axon and operate independently. HII horizontal cell

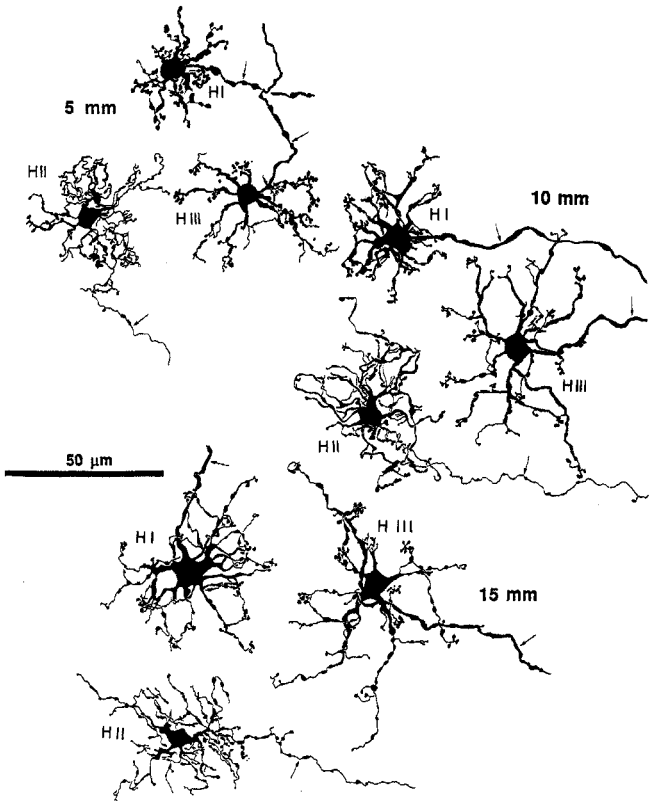

Figure 4: Horizontal cell morphology.
Golgi-stained human horizontal cells showing HI, HII and HIII cell morphology at retinal eccentricities of 5, 10 and 15 mm. Axons are marked with arrows. From Kolb et al., 1994.

dendrites densely contact S cones and more sparsely contact L and M cones. The HII cell has an axon that does not form a terminal arbor like the HI, but sparsely contacts S cones. The HIII horizontal cell is similar to the HI type, but has a slightly larger dendritic tree that contacts more cones.

Horizontal cell dendrites extend into the cone pedicle invagination on either side of ON bipolar cell dendrites. Like OFF bipolar cells, horizontal cells express ionotropic AMPA/Kainate type glutamate receptors that produce a depolarizing response to glutamate (Calkins, 2005). Like cones, horizontal cells are depolarized in darkness and hyperpolarize in response to light. When a single horizontal cell is injected with dye, it

diffuses to many of its neighboring horizontal cells (Kaneko, 1971; Kaneko and Stuart, 1984). This extensive tracer coupling is mediated by gap junctions between the overlapping dendrites of horizontal cells (Janssen-Bienhold et al., 2001; Massey et al., 2003; O'Brien et al., 2006). Electrical signals generated in one horizontal cell can therefore pass to other horizontal cells in its vicinity and horizontal cell receptive fields are much larger than their dendritic fields (Naka and Rushton, 1967; Norton et al., 1968; Kaneko, 1971; Packer and Dacey, 2002). Horizontal cells provide lateral feedback between cones over large retinal areas, and the coupled network of horizontal cells extends the retinal area over which this lateral feedback operates. The function and mechanism of horizontal cell feedback is discussed in detail below.

Amacrine cells

Amacrine cells extend dendrites into the IPL and are presynaptic to bipolar cells and other amacrine cells and are postsynaptic to bipolar cells, amacrine cells and ganglion cells (Fig 5). Like horizontal cells, their dendrites serve as both input and output structures. Amacrine cells are the most morphologically diverse retinal cell class, and can be divided into ~30 morphological subtypes, the majority of which are not understood functionally (Mariani, 1990). They receive excitatory glutamatergic inputs from bipolar cells and produce mainly inhibitory output. Subtypes of amacrine cells preferentially produce either the inhibitory neurotransmitter GABA or glycine (Mariani, 1989). Some

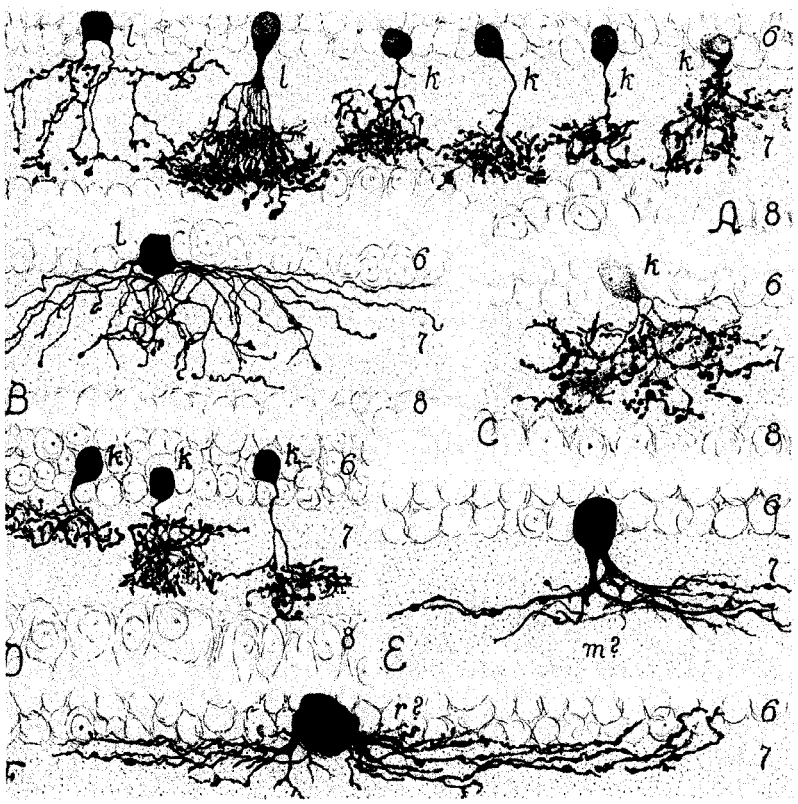

Figure 5: Amacrine cell morphology.
Golgi stained amacrine cells from macaque retina. Note the morphological diversity in density, lateral extent, and stratification in the IPL of the dendrites. From Polyak, 1941.

amacrine cell types use other neurotransmitters, such as the starburst amacrine cell, which synthesizes and releases acetylcholine or the dopaminergic amacrine cell, which produces dopamine. Other amacrine cells, such as the AII type, pass electrical signals directly to ganglion cells via gap junctions.

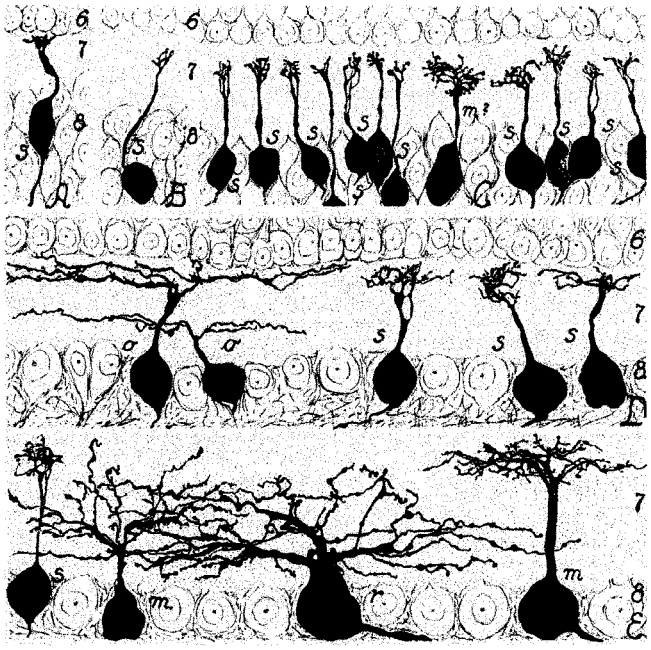

Figure 6: Ganglion cell morphology.
Golgi stained ganglion cells of macaque retina. Note the diversity of cell body size, lateral and vertical dendritie extent, and dendritic stratification in the IPL. From Polyak, 1941.

Ganglion Cells

Ganglion cell bodies occupy the ganglion cell layer and extend dendrites into the IPL (Fig 6). Their axons collectively form the optic nerve, which leaves the eye and projects to the lateral geniculate nucleus of the thalamus and other targets in the brain. They receive excitatory input from bipolar cells and predominantly inhibitory input from amacrine cells. In the primate retina there are ~ 20 ganglion cell types distinguished by their morphological and physiological properties, and by their projection targets in the brain. Ganglion cells exhibit complex response properties such as preference for stimuli moving in a particular direction, or preference for specific wavelengths of light.

Axon-bearing amacrine cells

"Amacrine" means lacking long processes, and amacrine cells were so named by Ramon Y Cajal because the majority of them have only dendrites that serve as both input and output structures. Even Cajal, however, appreciated that there were exceptions. Cells he called association amacrine cells had the characteristics of other amacrine cells, but had long, thin, axon-like processes that extended laterally for long distances within the retina. Modern studies have catalogued a number of amacrine cell types in the retinas of multiple species that have both dendritic and axonal compartments (Dacey, 1988, 1989, 1990; Famiglietti, 1992a, 1992c, 1992b; Volgyi et al., 2001; Witkovsky, 2004).

The A1 axon-bearing amacrine cells of the macaque monkey retina have large (15-20 μm in diameter) cell bodies found in the inner nuclear layer, and also in the ganglion cell layer and in the inner plexiform layer. These dispersed cell bodies nonetheless form a single population of cells. A1 cells have dendrites that are thick, spiny and highly branched, extending symmetrically ~200 μm from the soma in the peripheral retina and stratifying diffusely in both the ON and OFF sublayers of the IPL (Fig 7). Multiple (1-4) axons arise from the soma and proximal dendrites forming an arborization that extends away from the dendritic tree over 4 mm in the IPL. The axons are thin, sparsely branching and along their length are swellings that resemble presynaptic boutons (Fig 7, Dacey, 1989). Five polyaxonal cells (PA1-5) have been

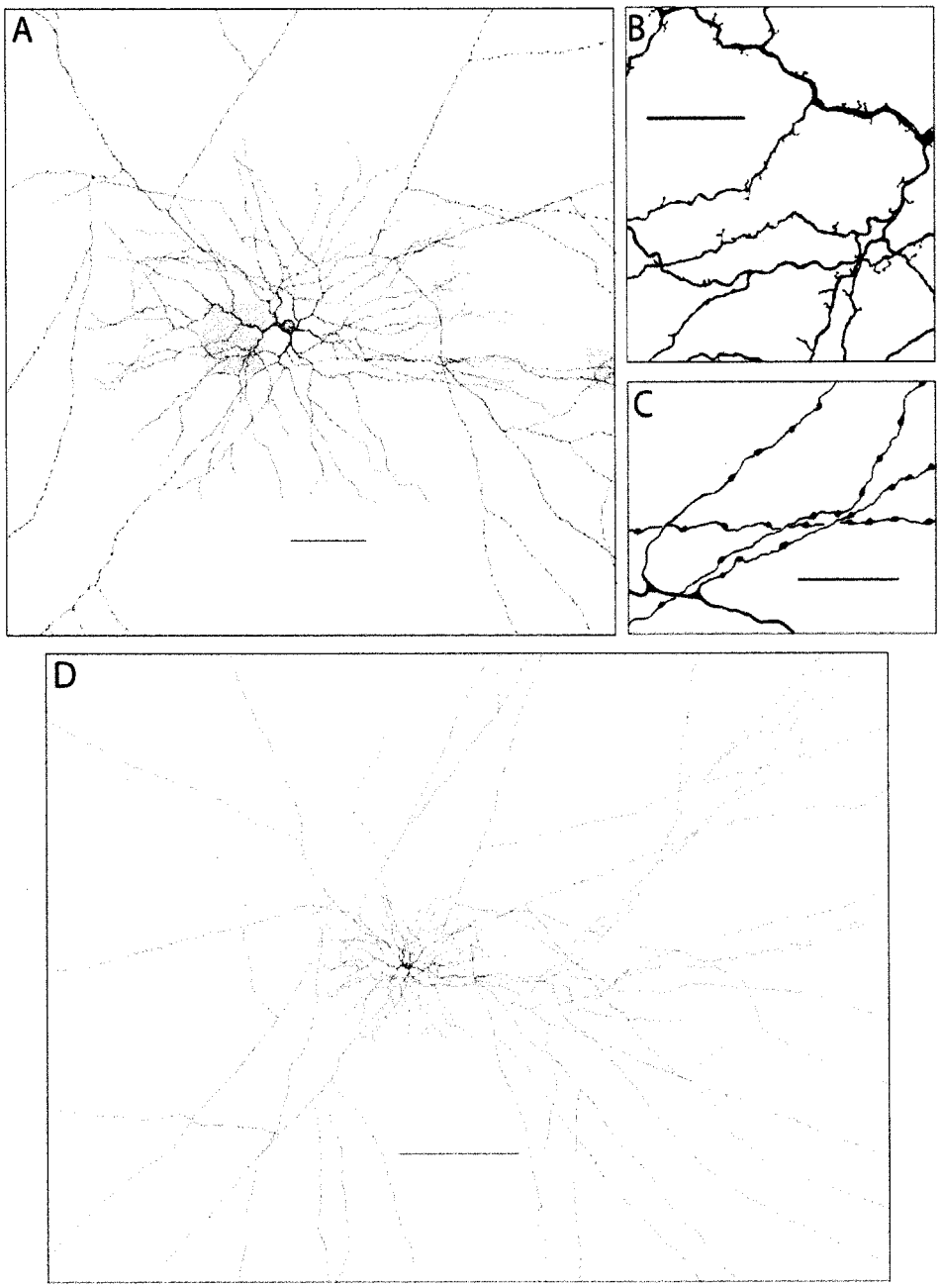

Fig 7: A1 amacrine cell morphology
A: A camera lucida tracing of a Neurobiotin filled A1 amacrine cell. The dendritic tree and proximal axons can be seen. Scale bar = 100 μm. **B:** A high magnification view of the dendritic tree from the proximal shaded area in A. Dendrites are thick, spiny and moderately branched. Scale bar = 25 μm. **C:** A high magnification view of the axonal tree from the distal shaded area in A. Axons are thin, sparsely branching, and have bouton-like swellings along their length. Scale bar = 25 μm. **D:** Low magnification image showing the axonal arbor. Scale bar = 400 μm.

identified in the rabbit retina, distinguished by their morphological and physiological properties (Famiglietti, 1992a, 1992c, 1992b; Volgyi et al., 2001). The PA1 cell type most closely resembles the primate A1 cell. It also has large cell bodies found in the IPL, GCL and INL, spiny dendrites stratified diffusely in the center of the IPL and thin, axonal projections from the soma and proximal dendrites (Famiglietti, 1992a, 1992b; Volgyi et al., 2001). Both the A1 and the PA1 cells show extensive tracer coupling to neighboring homologous amacrine cell types, and to other heterologous amacrine and ganglion cell types (Stafford and Dacey, 1997; Wright and Vaney, 2004).

The only electron microscopic study of an axon-bearing amacrine cell was of a single PA2 type cell in the rabbit retina (Famiglietti, 1992c). The dendrites received synaptic input predominantly from other amacrine cells, but also sparsely from bipolar cells. Vesicles were visible in the dendrites but there were no apparent presynaptic structures. Only the axon initial segment was examined but the cytoskeletal components visible were markedly different than those of the dendrites and more consistent with traditional axonal structure.

Sharp electrode recordings from A1 amacrine cells in the primate retina showed that they depolarize transiently at both the onset and offset of a light stimulus, and that they fire action potentials. Their receptive fields were also mapped with small spots and bars of light and were found to be approximately the same size as their dendritic field (Stafford and Dacey, 1997). Similar recordings from rabbit axon-bearing amacrine cells show that the PA1, PA2 and PA3 type have similar transient ON-OFF light responses, while PA4 and PA5 cells have only ON responses. All five types fire action potentials (Volgyi et al., 2001). The receptive field of the PA1 cell was mapped with spots of

increasing diameter, and it was similar in to the dendritic field, and also had a weakly inhibitory surround. Whole-cell voltage clamp recordings from two rabbit axon-bearing amacrine cells showed that they fire action potentials at a rate proportion to membrane potential depolarizations caused by somatic current injection, and that light-evoked inward currents were antagonized by an inhibitory surround (Taylor, 1996).

The fact that axon-bearing amacrine cells have axons and fire action potentials, and that their receptive fields, when measured, have approximated the size of their dendritic fields and not their axonal fields, has lead to the hypothesis that they receive input to their dendrites, and that their axons propagate a long-range output signal across the retina (Dacey, 1989). The majority of amacrine cells are inhibitory, and large amacrine cell bodies resembling A1 cell bodies have been positively stained for GABA synthesizing enzymes, suggesting that this output is inhibitory (Mariani et al., 1987). Because A1 axonal arbors are sparsely branching, an individual axon has very few potential contacts with a single postsynaptic cell, and therefore likely provides very weak inhibitory input. However, the axonal processes of A1 amacrine cells as a group, due to their large and overlapping axonal arbors could have a strong effect if activated simultaneously. It was therefore proposed that axon-bearing amacrine cells mediate inhibition in the retina in response to global retinal stimulation. During saccades, for example, when the entire visual world is shifted on the retina, our visual perception is inhibited (Burr, 2004). That global shift of the visual scene could simultaneously activate many axon-bearing amacrine cells, which are well suited to respond to moving stimuli due to their transient ON-OFF light responses, and their combined action could inhibit postsynaptic ganglion cells. There is evidence that global retinal stimuli do inhibit

ganglion cells consistent with this hypothesis. Specific rabbit ganglion cell types receive inhibitory input when presented with movies of natural scenes that shift with saccade-like motion (Roska and Werblin, 2003). These ganglion cell types have dendrites that stratify in the center of the IPL, where axon-bearing amacrine cell axons stratify. The inhibitory input is also blocked by tetrodotoxin, which blocks the action potentials that presumably mediate output from axon-bearing cells and also by picrotoxin which blocks GABAergic neurotransmission. Similarly, when presented with moving gratings outside of their classical receptive fields, specific rabbit and salamander ganglion cell types recorded on a multi-electrode array are inhibited at times when axon-bearing amacrine cells recorded simultaneously with sharp electrodes are depolarized (Olveczky et al., 2003). Axon-bearing amacrine cells have in addition been suggested to participate in dynamic regulation of ganglion cell receptive fields in response to novel visual environments (Hosoya et al., 2005), and in inverting ON and OFF light responses in retinal ganglion cells (Geffen et al., 2007).

In chapter 1 of this dissertation, I will describe pharmacological experiments that examine how the receptive field of the A1 amacrine cell is formed, and whether its action potentials represent an output signal. I will also describe imaging experiments that show that action potentials propagate throughout the axons, consistent with current hypotheses of A1 amacrine cell function.

Horizontal cell feedback and surround generation

An ON center parasol ganglion cell is excited strongly at the onset of a small spot, but weakly at the onset of a large spot. This is the classic receptive field property of many cells in the retina and early visual system called center-surround antagonism (Kuffler, 1953). It is thought that the center response is generated by direct bipolar cell input to ganglion cell dendrites, which is antagonized by lateral inhibitory circuits in the retina. Because of their minimal response to large stimuli, cells with center-surround receptive fields do not respond strongly to global changes in retinal luminance, but rather respond to local features in the visual scene such as small spots or light-dark borders. The lateral inhibition responsible for surround generation must be mediated by either horizontal cells in the outer retina or amacrine cells in the inner retina. Pharmacological studies from cat and rabbit retina have been equivocal as to which of these systems is primarily responsible for surround generation. Several studies have shown that blockers of GABA receptors and glycine receptors, which preferentially attenuate amacrine cell mediated lateral feedback in the inner retina have little effect on the surrounds of ganglion cells (Daw and Ariel, 1981; Frishman and Linsenmeier, 1982; Bolz et al., 1985), and that the sodium channel blocker tetrodotoxin, which would be expected to affect the output of long-range, spiking amacrine cells also has little effect on ganglion cell surrounds (Bloomfield, 1996). Other studies, however, have found that PTX and TTX attenuate surround inhibition measured in excitatory currents of ganglion cells (Taylor, 1999; Flores-Herr et al., 2001). In the primate retina, only one study has examined the pharmacology of ganglion cell surrounds, and is consistent with an outer retinal mechanism of surround generation. Primate parasol ganglion cell surrounds are

insensitive to picrotoxin, strychnine and TTX, but are sensitive to carbenoxolone and cobalt, which block horizontal cell feedback to cones (McMahon et al., 2004). In addition, primate cones themselves posses antagonistic surrounds, which must be generated by horizontal cell feedback (Baylor et al., 1971; Ambrose and Hayhoe, 1980; Verweij et al., 2003). Together, these results suggest that in different species and under different conditions amacrine cell and horizontal cell mediated lateral inhibition contribute differentially to surround formation. In the light-adapted primate retina, however, evidence is consistent with horizontal cell feedback as the major contributor to ganglion cell surrounds.

Horizontal cells are postsynaptic to cones in the cone pedicle and are depolarized by glutamate released from cones in darkness. In response to light, decreased cone glutamate release causes horizontal cells to hyperpolarize, and this hyperpolarization leads to a depolarization in cones that opposes the original light induced hyperpolarization. The mechanism of the synaptic feedback from horizontal cells to cones has been studied extensively, particularly in goldfish retina, but remains controversial. Initial evidence suggested that feedback was GABAergic (reviewed in Wu, 1992; Kamermans and Spekreijse, 1999). According to this hypothesis, in darkness depolarized horizontal cells constantly release GABA. With an increase in light intensity, horizontal cells hyperpolarize and stop releasing GABA and this relief of inhibition causes a depolarization in cones. Consistent with this picture, goldfish cones express GABA receptors measured with immunohistological (Yazulla et al., 1989) and physiological methods (Verweij et al., 1998). Goldfish horizontal cells express the GABA synthesizing enzyme GAD and GABA itself (Marc et al., 1978; Yazulla and

Brecha, 1980) and isolated horizontal cells can release GABA (Ayoub and Lam, 1984). The surround has also been shown to be sensitive to Cl^-, consistent with the involvement of a GABA-gated Cl^- conductance (Kaneko and Tachibana, 1986). However, pharmacological blockade of GABA receptors does not consistently abolish goldfish horizontal cell feedback or the surrounds of cones (Perlman and Normann, 1990; Verweij et al., 1996; Verweij et al., 1998) and the depolarizing surround response in cones is not completely consistent with a GABAergic mechanism (Verweij et al., 1996). Horizontal cells also do not contain vesicles appropriately positioned to be presynaptic to cone axon terminals. In the primate retina, horizontal cells also express GAD (Vardi et al., 1994) and cones do express GABA receptors, though not at axonal locations that are directly apposed to horizontal cells (Verweij et al., 1996). However, consistent with results from goldfish, GABAergic antagonists do not block feedback to cones (Verweij et al., 2003), or other measures of horizontal cell feedback in primate retina (McMahon et al., 2004). These results in both goldfish and primate, in addition to results from other species, cast doubt on the GABAergic hypothesis of horizontal cell feedback.

Recently it has been shown that horizontal cell feedback causes a shift in the activation curve of cone calcium channels that could account for feedback (Verweij et al., 1996). By shifting the activation curve to more negative potentials, feedback causes more calcium channels to open, leading to a depolarization that opposes the light-induced hyperpolarization in cones, and also increases calcium influx and thus glutamate release. Two alternative hypotheses to explain how horizontal cell hyperpolarization could shift the cone calcium channel activation curve have risen to prominence recently. The first is the ephaptic hypothesis, whereby current flow through hemichannels (half gap junctions)

on horizontal cell dendritic tips in the cone pedicle allow the horizontal cell membrane potential to change the apparent extracellular voltage sensed by cone calcium channels (Byzov and Shura-Bura, 1986; Kamermans et al., 2001). This hypothesis is supported primarily by the sensitivity of horizontal cell feedback in goldfish to carbenoxolone, a gap junction blocker (Kamermans et al., 2001). Measures of horizontal cell feedback in the primate retina are also sensitive to carbenoxolone (McMahon et al., 2004; Packer and Dacey, 2005). The second is the pH hypothesis, whereby horizontal cell hyperpolarization causes an increase in the extracellular pH of the synaptic cleft that releases inhibition of cone calcium channels by protons (Barnes and Bui, 1991; Barnes, 2003). This hypothesis is supported by the sensitivity of horizontal cell feedback to exogenous pH buffers, such as HEPES (Hirasawa and Kaneko, 2003; Vessey et al., 2005a). The mechanism by which this pH change is accomplished is unknown.

In the second part of this dissertation I will describe experiments testing the effect of HEPES and other pH buffers on two feedback-dependent phenomena in the primate retina: the surrounds of ganglion cells and the slow depolarization of horizontal cells.

Blue-yellow opponency in small bistratified ganglion cells.

Our perception of color begins with the absorption of photons by the cone photoreceptors. Human cones express one of three opsins that are maximally sensitive at different wavelengths of light. From the output of only these three cone types, the nervous system generates a representation of the myriad colors that we can perceive. Because individual cones have broad spectral tuning curves, a single photoreceptor cannot provide information about the wavelength of light that it absorbs, only that it has

absorbed a photon. To generate our perception of color, the nervous system compares the output of different cone classes in a process called opponency, in which downstream cells receive antagonistic input from different cone types. This is not only essential, based upon the broad spectral tuning of cones, but is also efficient. If cone types had narrow tuning curves and were more wavelength-specific, many more cone types would be needed to sample the whole visible spectrum of light. There are neural pathways that compare the output of L cones to M cones in the red-green axis of color vision and pathways that compare the output of S cones to both L and M cones in the blue-yellow axis (Dacey, 1996). Early recordings in the lateral geniculate nucleus, the thalamic nucleus (LGN) where retinal ganglion cell axons terminate, revealed cells that responded to the onset of a blue light and the offset of a yellow light (De Valois et al., 1958). These two signals oppose each other, such that when the cells receive equal input from S and L and M cones, their response is minimal. Subsequent recordings in LGN revealed that the blue ON-yellow OFF cells had spatially coextensive type II receptive field organization, meaning the blue ON and yellow OFF receptive fields occupy the same retinal space (Wiesel and Hubel, 1966). This is in contrast to the concentric center-surround type I receptive field organization (as described above). The specific primate retinal ganglion cell type that displays the blue ON-yellow OFF physiology was discovered to be the small bistratified cell (Dacey, 1993; Dacey and Lee, 1994). The small bistratified cell has dendrites in both the ON and OFF sublayers of the inner plexiform layer. This led to the hypothesis that it received input to its inner dendrites from ON bipolar cells connected to S cones and input its outer dendrites from OFF bipolar cells connected to L and M cones. This would create both the blue ON-yellow OFF light responses and the type II receptive

field. Electron microscopy has subsequently been performed on the small bistratified cell that has confirmed some aspects of this hypothesized circuitry, but questioned others. In the macaque fovea, small bistratified cells do receive input from bipolar cells that almost exclusively contact S cones to their inner dendrites and L+M cone bipolar cells to their outer dendrites. They also receive amacrine cell input to both inner and outer dendrites. Their inner dendrites receive ~ 33 bipolar contacts and ~10 amacrine cell contacts, and their outer dendrites receive ~ 14 bipolar cell contacts and ~ 10 amacrine cell contacts (Calkins et al., 1998). In the periphery of the marmoset retina, small bistratified cells also receive bipolar cell and amacrine cell input to their inner and outer dendrites, but the percentage of amacrine cell input is far greater. The cells receive ~84 % total amacrine cell input, and of the remaining 16 % bipolar cell input, only about 1 % is to the outer dendrites (Ghosh and Grunert, 1999). Both of these studies confirm that the small bistratified cell does receive appropriate bipolar cell input to its dendrites. However, the fact that in both cases, and especially in the marmoset, there is substantially less bipolar cell input to the outer dendrites could be inconsistent with the simple ON-OFF model of small bistratified cell circuitry. For the S ON and L+M OFF responses to be equal and opponent, the OFF bipolar cell synapses to the outer trees would have to have a stronger gain than the ON bipolar cell synapses to the inner tree. Alternatively, the yellow OFF response could be generated by another mechanism. One possibility is that inhibitory inputs from amacrine cells could invert an L+M ON response to an L+M OFF response. Another possibility is the HII horizontal cell, which contacts and receives input from all three cone types could provide antagonistic feedback from L and M cones to S cones, creating an L+M surround in S cones and S ON bipolar cells. The HII cell was

initially rejected as mediating opponency because it receives similar input from all three cone types, and thus does not itself display an opponent response (Dacey et al., 1996). In addition, an L+M surround would be expected to produce a type I receptive field in the small bistratified cell, rather than the type II receptive field, which is observed.

In the final part of this dissertation I will describe experiments that test the ON-OFF model and these alternative models of blue-yellow opponency in the small bistratified ganglion cell.

Chapter 1: Functional Polarity of A1 Amacrine Cells

Introduction

It is well established that a number of large field amacrine cell types possess morphologically distinct dendritic and axonal components (Dacey, 1988, 1989, 1990; Famiglietti, 1992a, 1992c, 1992b; Volgyi et al., 2001; Witkovsky, 2004) but much less is known about the physiological significance of these anatomical structures. The A1 axon-bearing amacrine cell of the macaque monkey retina is an example of such a cell type (Fig 7). A1 cell dendrites are thick, spiny and highly branched (Fig 7B), extending symmetrically ~200 μm from the soma and stratifying diffusely in the ON and OFF sublayers of the inner plexiform layer (IPL). Multiple (1-4) axons arise from the soma and proximal dendrites forming an arborization that extends away from the dendritic tree over 4 mm in the IPL. The axons are thin, sparsely branching and along their length are swellings that resemble presynaptic boutons (Fig 7C, Dacey, 1989). Intracellular recordings from A1 amacrine cells, and similar amacrine cells in rabbit retina (Taylor, 1996; Volgyi et al., 2001) revealed that they depolarize transiently and fire action potentials at light onset and offset. The A1 receptive field mapped with small spots and bars is approximately the same size as its dendritic field (Stafford and Dacey, 1997) leading to the hypothesis that A1 cells receive inputs to their dendrites causing depolarization and initiation of action potentials which then propagate down the axons and across the retina. Because their arborizations are so large, A1 cell axons collectively form a network that extensively covers the retina (estimates are as high as 1000 mm of axon/mm^2 retina) (Dacey, 1989; Wright and Vaney, 2004), suggesting that they serve a global function in the visual processing.

Global retinal stimuli can effect ganglion cells when presented outside of their classical receptive fields (Werblin, 1972; Kruger et al., 1975; Solomon et al., 2006). Recently two studies specifically invoked axon-bearing amacrine cells as mediators of long-range inhibition of ganglion cells in response to global image motion. Roska and Werblin (Roska and Werblin, 2003) presented movies of natural images that shifted with saccade-like motion and found that this motion inhibited specific ganglion cell types whose dendrites stratified in the center of the IPL. They also showed that antagonists of GABA receptors and voltage-gated sodium channels could block the shift-induced inhibition, consistent with axon-bearing amacrine cell involvement. Olveczky et al. (Olveczky et al., 2003) showed that a grating moved outside of a ganglion cell's receptive field could inhibit responses to a grating moved within a cell's receptive field. They recorded from axon-bearing amacrine cells and showed that they depolarized at times when action potentials were inhibited in ganglion cells recorded simultaneously on a multi-electrode array.

These hypotheses of axon-bearing amacrine cell function rest on the assumption that the axons are output structures that transmit spikes across the retina. Here we test this assumption in several ways. We perform detailed measurements of the spatial receptive field of A1 amacrine cells using spot and annulus stimuli better suited to measure center-surround structure than the small spots and bars previously used, and compare the physiological receptive field to the morphological dendritic and axonal fields. We find that the A1 does respond to light stimuli beyond its dendritic field but we present pharmacological evidence that these responses originate from a surround mechanism not associated with the axons. We show that blocking A1 action potentials has no significant

effect on receptive field properties, consistent with the axons carrying an output signal. In addition, we image light-evoked calcium transients in the axons of A1 cells and show that voltage gated sodium channels are necessary for a light induced axonal calcium increase, consistent with the hypothesis that action potentials propagate through the axonal arbor.

Methods

Tissue Preparation

Tissue was prepared as previously described (Dacey et al., 2000b). In brief, *Macaca nemestrina* or *fascicularis* retinas were obtained from the tissue distribution program of the Washington National Primate Research Center at the University of Washington. Under deep barbiturate anesthesia eyes were enucleated and hemisected to remove the anterior pole including the lens and vitreous humor. The retina, choroid and pigment epithelium were dissected as a unit from the sclera. Radial cuts were made to flatten the retina and it was fixed to a recording chamber with poly-L-lysine, vitreal side up. The chamber was mounted in an upright microscope for receptive field studies or a two-photon microscope for imaging studies. The retina was superfused with oxygenated Ames medium and maintained at 36 °C. Pharmacological agents were mixed with Ames medium and applied to the bath superfusion. All pharmacological agents were obtained from Sigma (St Louis, MO).

Electrical Recording

Glass microelectrodes (R = 250-500 MΩ) were filled with 2% Neurobiotin and 2% pyranine in 1M KCl. Retinal somata were stained with the vital dye acridine orange (several drops of 50 μM solution were added to the bath) and visualized with fluorescence episcopic illumination simultaneously with the microelectrode. A1 amacrine cell bodies were targeted based upon their large (15-20 μm), round somas located in the center of the IPL or in the INL, and identity was confirmed after iontophoresis of pyranine allowed the examination of dendritic morphology in vitro. The electrode tip was positioned next to the soma and penetration was achieved using the amplifier's buzz feature. Intracellular voltage was amplified (Axoprobe 2B, Axon Instruments, Sunnyvale, CA) and digitized at 10 KHz. Data acquisition was controlled by custom software.

Tissue Processing

Retinas were processed to recover the morphology of cells filled with Neurobiotin. At the end of the experiment retinas were dissected from the pigment epithelium and choroid, fixed in 4% paraformaldehyde in 0.1 M phosphate buffer for 2hr, rinsed overnight and placed in a buffered solution of 0.1% Triton X-100 containing avidin-biotin-horseradish-peroxidase complexes (Vector Laboratories, Burlingam, CA) for 8hr. Retinas were then rinsed overnight, and horseradish-peroxidase histochemistry was performed with the use of diaminobenzidine (Kirkegaard & Perry Laboratories, Gaithersberg, MD) as the chromogen. Processed retinas were mounted on glass slides in a solution of polyvinyl alcohol and glycerol and stored at 4 °C.

Visual Stimuli

Visual stimuli were generated by a digital projector (VistaGRAPHX 2500, Christie Digital, Cypress, CA) controlled by custom software through a VSG3 stimulus generator (Cambridge Research Systems, England)(Packer et al., 2001). Stimuli were focused through a 4x objective onto the retina. The retinal area covered by the stimulus was 2.96 X 2.22 mm. All stimuli used for receptive field measurements were white spots and annuli centered over the cell's receptive field which were modulated above and below a mid-photopic background luminance (L_{BKG}, estimated photon flux = 3.4 X 10^5 photons/μm^2 /second) at 100% contrast (contrast = L_{MAX}-L_{BKG}/L_{BKG}) at 2.03 Hz. A small test flash was first used to center the stimulus over the receptive field by manually moving it to elicit a maximum response. Twenty four light flashes were presented to the cell and the responses were averaged and quantified by taking the maximum amplitude or the area of the ON and OFF components of the voltage response separately or averaged together. Statistical significance was determined by performing a Student's T-test, with a p value of less than 0.05 indicating significance.

Calcium Imaging

Retinas were mounted on a custom-built two-photon microscope (Denk *et al.*, 1990). Fluorescence was excited by a mode-locked Ti:S laser and emission was band pass filtered (535 ± 25 nm) and monitored with a photomultiplier tube. Electrodes were filled with 5 mM Oregon Green BAPTA-1 (OGB-1, Invitrogen, Carlsbad, CA) in 1 M KAcetate. Cells were labeled with acridine orange and recordings obtained as described above. Cells were allowed to fill with OGB for 30 to 90 min with negative current (50-

100 pA) applied to the electrode. Because of the long time necessary to fill the axons, in some, but not all cells the electrical recording deteriorated by the time the axons were filled. In these cases the electrode was pulled off of the cell and it was allowed to recover for 30-60 min before imaging. Axons were easily identified by their extension >500 μm from the soma. Fluorescence was collected in line scan mode at 2 ms/line. During imaging A1 cells were stimulated by a red LED (630 nm, 10 cd @ 20 mA, 15° viewing angle) that was placed above the retina and provided diffuse illumination. Responses to the LED were similar to responses to the digital projector used for receptive field studies. Raw fluorescence data was background-subtracted and the stimulus-evoked change in fluorescence intensity (F(t)) was scaled by the pre-stimulus intensity (F(0)) to give the ratio ΔF/F (ΔF/F = F(t)-F(0)/F(0)). Custom software controlled and coordinated imaging and physiological data collection. Morphological reconstructions of cells were obtained by taking image z-stacks at different positions, collapsing them and manually aligning the resulting tiles into a montage using ImageJ (NIH, rsb.info.nih.gov/ij).

Results

A1 Center-surround receptive field structure

Primate cone bipolar cells have center-surround receptive field structure (Dacey et al., 2000a). ON cone bipolar cells have an ON center response that is antagonized by simultaneous surround stimulation. When stimulated in isolation, the surround produces and OFF response. The opposite is true for an OFF cone bipolar cell. With dendrites in both ON and OFF sublamina of the IPL, A1 amacrine cells can receive input from both ON and OFF bipolar cells and should thus inherit centers and surrounds of both types. In

previous receptive field studies using small spots and bars of light an antagonistic surround was found in some rabbit polyaxonal amacrine cells (Volgyi et al., 2001), but not in primate A1 amacrine cells (Stafford and Dacey, 1997). However, these small stimuli are not ideally suited to measure center-surround interactions due to the large size and low gain of the surround. To test further for the presence of an antagonistic surround linked to the ON and/or OFF responses in A1 cells the spatial receptive field was mapped using spot and annular stimuli.

Figure 8A shows an example of A1 cell responses to spots of light at several diameters. The response to a 2000 μm spot (bottom) is smaller than the response to a 450 μm spot (middle), indicating the presence of an antagonistic surround. Figure 8B shows the peak ON and OFF response amplitude as a function of spot diameter. As spot diameter increases the response reaches a maximum after which the peak voltage decreases to 0.82 ± .03 (ON) and 0.78 ± .02 (OFF) of its maximum (n=28). Figure 8C shows the area under the voltage response as a function of spot diameter. As spot diameter increases the area reaches a maximum after which it decreases to 0.46 ± 0.04 (ON) and 0.439 ± 0.04 (OFF) of its maximum (n=28). The more substantial surround antagonism as measured by response area suggests that the surround's primary effect is to make the response more transient. As an estimate of the center size we measured the spot size that elicited the maximum response area (494 ± 68 μm (ON) and 472 ± 64 μm (OFF), n=28). This is approximately the size of the A1 dendritic tree diameter as previously reported (300-500 μm in the periphery (Dacey, 1989)).

To examine the surround in isolation we presented A1 cells with annuli. Figure 8D shows the response of an A1 cell to several annuli with fixed outer diameters of

Figure 8: A1 Spatial Receptive Field.
A: Responses to 72 (top), 450 (middle) and 2000 (bottom) μm spots of light (stimulus trace below). All stimuli, unless otherwise noted, are flashed on and off at 250 ms intervals. Top scale bar = 4 mV, middle and bottom scale bars = 20 mV. **B:** The peak voltage response of the ON (open circles) and OFF (closed circles) components normalized to the maximum response amplitude, plotted against spot diameter, n=28 cells. Error bars in this and all figures represent the standard error of the mean (SEM). As spot size increases, the response amplitude increases to a maximum, after which it decreases, indicating the presence of an inhibitory surround. **C:** The area of the voltage response of the ON (open circles) and OFF (closed circles) responses normalized to the maximum response area, plotted against spot diameter (the area response function). The ON and OFF components have similar area response functions. The surround is more evident than in the peak voltage measurements, n=28. **D:** Responses to an annulus with 2000 μm outer diameter and 72 (top), 300 (middle) and 1200 (bottom) μm inner diameter (stimulus trace below). The 300 μm inner diameter annulus evokes fast and delayed (arrow) components. Top and middle scale bars = 20 mV, bottom scale bar = 4 mV. **E:** The peak voltage of the ON (open circles) and OFF (closed circles) responses normalized to the maximum response amplitude and plotted against annulus inner diameter. The outer diameter of the annulus was fixed at 2 mm. With small annulus inner diameter the center and surround antagonize each other to produce a diminished response. As the annulus inner diameter grows, the center is no longer stimulated and the surround is fully stimulated, yielding a larger response. As the annulus inner diameter grows further, the surround is stimulated less and the response decreases. n=27. **F:** The area of the of the ON (open circles) and OFF (closed circles) voltage responses normalized to the maximum area and plotted against annulus inner diameter (the annulus response function). n=27.

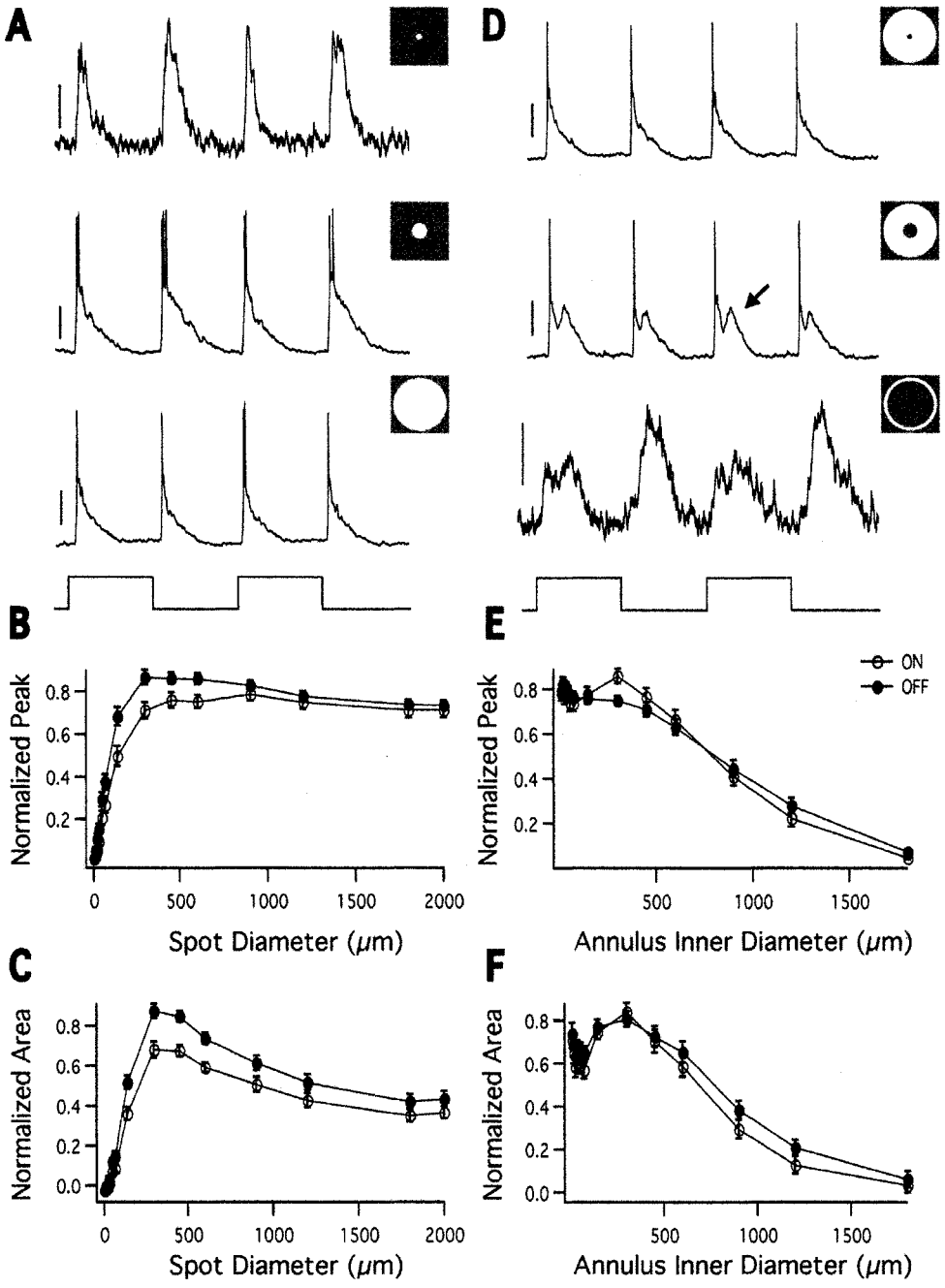
A
D
B
E
C
F
Normalized Peak
Normalized Area
Spot Diameter (μm)
Annulus Inner Diameter (μm)
ON
OFF
0
500
1000
1500
2000
0.2
0.4
0.6
0.8
0.0

2000 μm and increasing inner diameters. The cells respond to surround stimulation at light onset and offset. At larger annulus inner diameters, the response consists of a fast component and a delayed component. The delayed component, which was not always obvious, could be due to delayed input from the surround, electrical coupling to neighboring A1 cells, or complex interactions of the ON and OFF systems. Figure 8E shows the peak response of the ON and OFF components as a function of annulus inner diameter. The response initially decreases as center stimulation is removed. As the inner diameter increases further the response increases, as the center no longer antagonizes the surround and the surround dominates. The response then decreases as the surround is less stimulated, but was still measurable even with annulus inner diameters of 1200 μm and even occasionally 1800 μm. Figure 8F shows the response area as a function of annulus inner diameter. The shape of the curve is similar but as the surround is more evident in the area measurement, the initial decrease and increase are more exaggerated. As an arbitrary estimate of surround size we measured the point at which the annulus response function decreased to 50% of its maximum (675 ± 56 μm (ON) and 772 ± 57 (OFF), n=27).

These results show that the A1 receptive field center consists of ON and OFF components both of which are antagonized by surround stimulation. When stimulated in isolation, the surround produces ON and OFF responses. This could mean that the A1 receives input from ON and OFF bipolar cells, with OFF and ON surrounds, respectively.

Effect of L-AP4 on A1 receptive field

To examine further the retinal pathways that generate the ON and OFF responses of the center and surround, the receptive field properties of A1 cells were studied in the presence of L-(+)-2-Amino-4-phosphono-butyric acid (L-AP4), a compound that blocks the ON pathway (Slaughter and Miller, 1981). If the A1 is inheriting its surround from bipolar cells, abolishing ON bipolar cell input with L-AP4 should abolish the ON center and OFF surround, and leave the OFF center and ON surround inherited from the OFF bipolar cell intact. In the presence of 100 μM L-AP4 spots of light evoke a normal OFF response and no ON response at all spot sizes (Fig 3A, B). This is consistent with ON bipolar cell input generating ON center responses.

The OFF responses to spots up to ~ 300 μm are not affected by L-AP4. Blocking the ON pathway does, however, weaken the antagonism of the OFF response by larger diameter spots (Fig 9C). The OFF response to a 2000 micron spot is 0.36 ± 0.03 of maximum in control and 0.61 ± 0.07 of maximum in the presence of L-AP4 ($p = .012$, $n=5$). This indicates that OFF bipolar cell input generates the OFF center response, but that these responses are antagonized in part by a surround mechanism generated by the ON pathway.

L-AP4 blocks ON responses evoked by annuli with small but not large inner diameters (Fig 9D, E). This is consistent with the A1 inheriting its ON surround from OFF bipolar cell input. Annuli with small inner diameters evoke no response because the OFF center and ON surround of the OFF bipolar cells antagonize each other.

L-AP4 increased OFF responses to annuli with small inner diameters (Fig 9F), consistent with the decreased surround antagonism observed in response to large

Fig 9: Effect of L-AP4 on A1 receptive field
A: Responses to a 300 μm spot in the absence (black) and presence (red) of 100 μM L-AP4 (stimulus below traces). L-AP4 eliminates the ON component of the spot response, but the OFF component is unchanged. **B:** The area response function of the ON component of the light response in the absence (black) and presence (red) of L-AP4. L-AP4 eliminates the ON response at all spot sizes. n=4. **C:** The area response function of the OFF component of the light response in the absence (black) and presence (red) of L-AP4. In the presence of L-AP4 The OFF response to large spots is increased, indicating a decrease of surround antagonism. n=4. **D:** Responses to a 450 μm inner diameter annulus in the absence (black) and presence (red) of L-AP4 (stimulus trace below). In response to the annulus, both ON and OFF responses are evoked in the presence of L-AP4. Scale bars = 20 mV. **E:** The annulus response function of the ON component of the light response in the absence (black) and presence (red) of L-AP4. As the annulus inner diameter grows, the ON response returns to control levels, indicating it originates from the OFF system. n=4. **F:** The annulus response function of the OFF component of the light response in the absence (black) and presence (red) of L-AP4. The OFF response is elevated at small annulus inner diameters, indicating a decrease of surround antagonism. At larger annulus inner diameters, the OFF response is the same as control, indicating the OFF surround response originates from the OFF pathway. n=4.

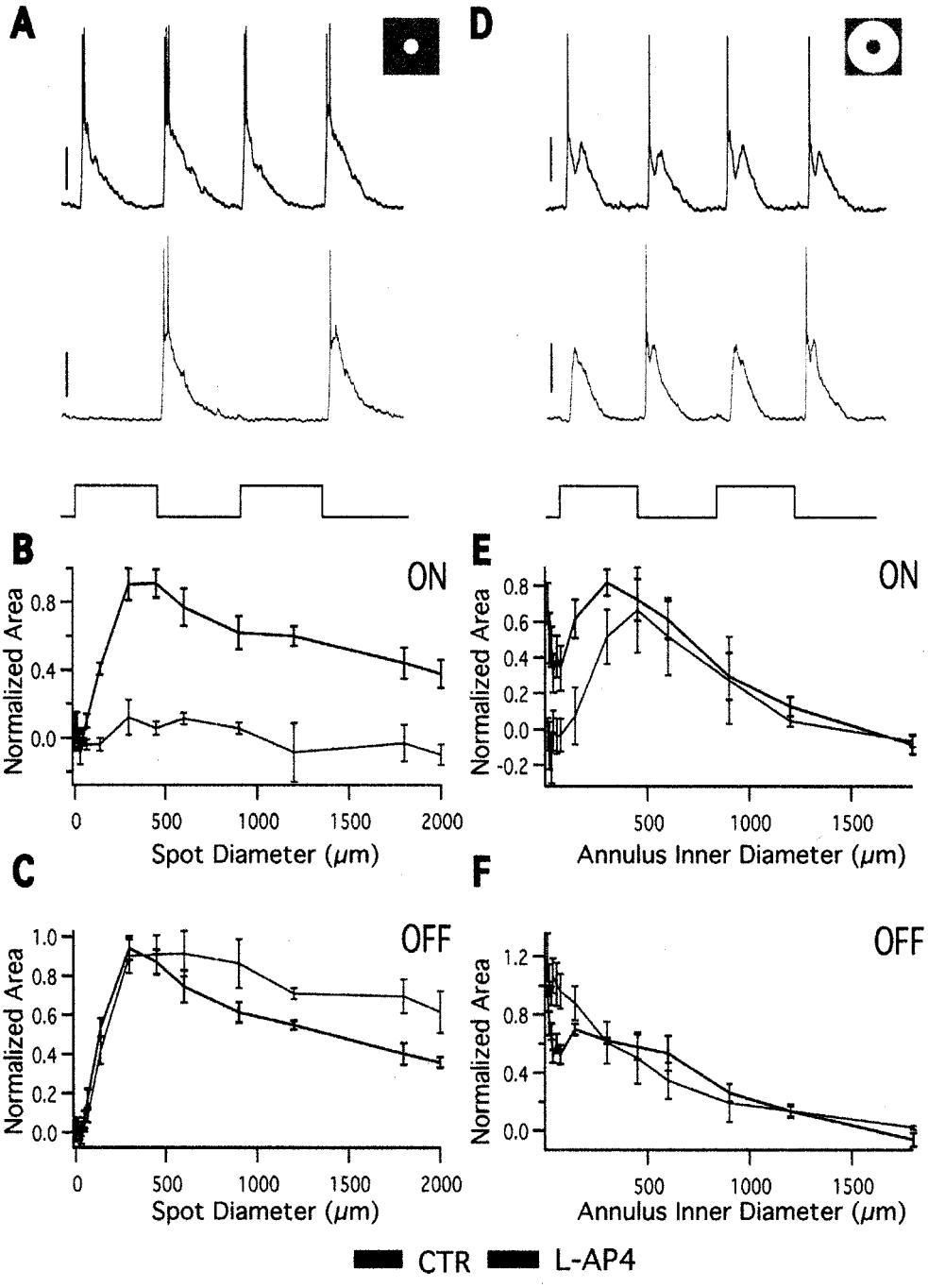
A
D
B
ON
Normalized Area
0.8
0.4
0.0
0
500
1000
1500
2000
Spot Diameter (μm)
E
ON
Normalized Area
0.8
0.6
0.4
0.2
0.0
-0.2
500
1000
1500
Annulus Inner Diameter (μm)
C
OFF
Normalized Area
1.0
0.8
0.6
0.4
0.2
0.0
0
500
1000
1500
2000
Spot Diameter (μm)
F
OFF
Normalized Area
1.2
0.8
0.4
0.0
500
1000
1500
Annulus Inner Diameter (μm)
CTR
L-AP4

spots (Fig 9C). However, OFF responses evoked by annuli with large inner diameters were not significantly affected by L-AP4. This is surprising because it means the A1 does not receive its OFF surround responses from ON bipolar cell input, and indicates that some other mechanism that is maintained in the presence of L-AP4 generates OFF surround responses. One possibility is that neighboring A1 cells, which show extensive tracer coupling (Dacey, 1989; Wright and Vaney, 2004), could pass their OFF center responses to the recorded cell via electric coupling. These response would appear as OFF surround responses.

Overall, these data are consistent with bipolar cell input being responsible for the A1 cell center-surround receptive field structure but do not support a pure separation of the ON and OFF pathways. The ON pathway appears to contribute some surround antagonism of the OFF center responses, and the OFF pathway appears to contribute to OFF surround responses.

Effect of picrotoxin on A1 receptive field

To test what role GABAergic inhibition plays in the A1 amacrine cell receptive field, specifically in the generation of the A1 antagonistic surround, we mapped the spatial receptive field in the presence of 100 μM picrotoxin (PTX) that blocks GABA A and C receptors. PTX increased the response amplitude at all spot (Fig 10A, B) and annulus (Fig 10C, D) sizes. However, the center size, surround size and surround antagonism were not significantly affected by PTX (Table 1). These results indicate that GABAergic inhibition participates in the retinal circuitry of the A1 cell but is not involved in surround antagonism.

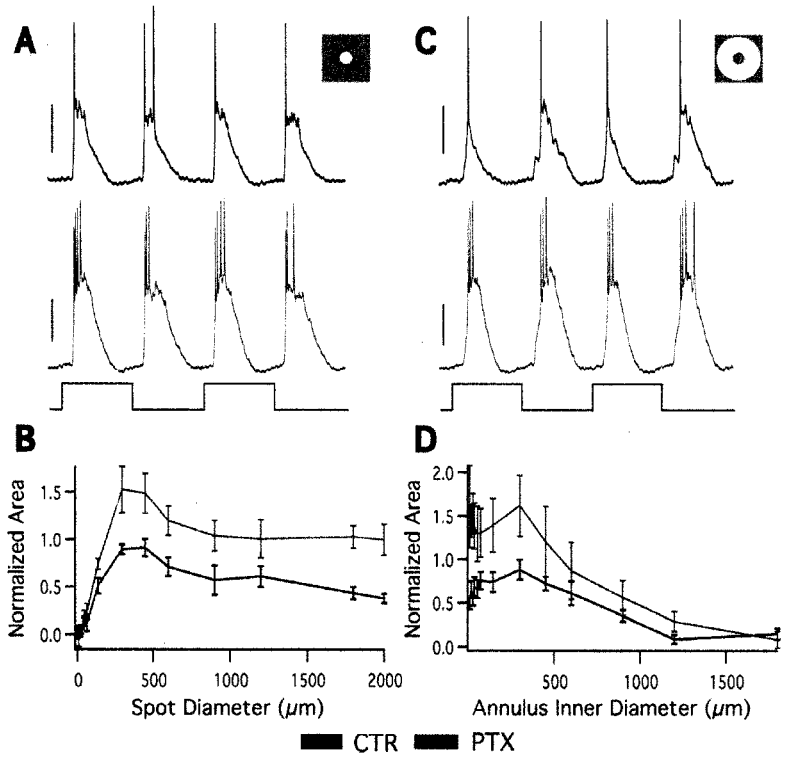

Fig 10: Effect of picrotoxin on A1 receptive field
A: Responses to a 450 μm spot in the absence (black) and presence (red) of 100 μM PTX (stimulus trace below). The picrotoxin response is larger than control. Scale bars = 10 mV. **B:** The averaged area response function in the absence (black) and presence (red) of PTX. PTX increases the response at all spot sizes, but surround antagonism is still present. n=4. **C:** Responses to a 450 μm inner diameter annulus in the absence (black) and presence (red) of PTX (stimulus trace below). Scale bars = 20 mV. **D:** The averaged annulus response function in the absence (black) and presence (red) of PTX. PTX increases the response at all annulus sizes, though the increase is predominantly at small annulus inner diameters. n=4.

Effect of tetrodotoxin on A1 receptive field

To test the hypothesis that action potentials serve an output function in A1 cells we mapped the spatial receptive field in the presence of 0.5 μM tetrodotoxin (TTX), which blocks the voltage gated sodium channels responsible for fast action potential generation. If action potentials are purely an output signal that propagates away from the

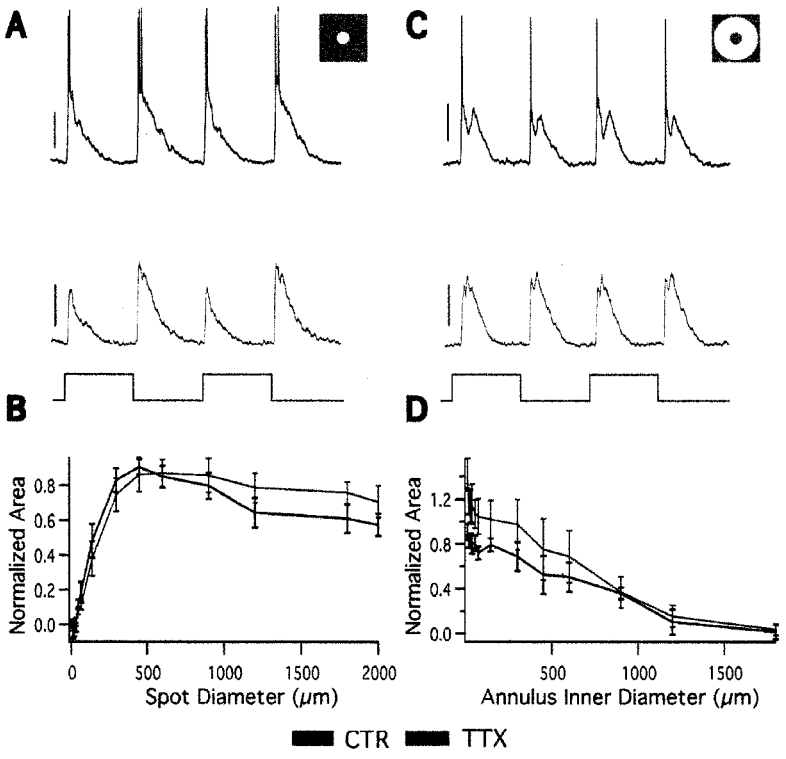

Fig 11: Effect of tetrodotoxin on A1 receptive field
A: Responses to a 450 μm spot of light in the absence (black and presence (red) of 0.5 μM TTX (stimulus trace below). TTX eliminates the action potentials but minimally effects light-evoked depolarizations. Scale bars = 20 mV. **B:** The average area response function in the absence (black) and presence (red) of TTX. TTX. n=5. **C:** Responses to a 450 μm inner diameter annulus in the absence (black) and presence (red) of TTX (stimulus trace below). Scale bars = 20 mV. **D:** The averaged annulus response function in the absence (black) and presence (red) of TTX. The responses in the surround are similar with and without TTX. n=5.

soma, TTX should not affect the receptive field size measurements. However, if the action potentials serve to propagate input to the soma along the axons, TTX should reduce the spatial receptive field size by eliminating responses that originate outside the dendritic field. Application of TTX completely abolished A1 fast action potentials, but had little effect on depolarizations (Fig 11A, C) or the receptive field properties (Fig 11B, D). Center size, surround size and surround antagonism were not significantly affected by

Table 1: Effects of PTX and TTX on A1 receptive field properties.

	Center Size (μm)	Surround Size (μm)	Surround Strength
CTR	413 ± 38	678 ± 94	0.34 ± 0.1
PTX	338 ± 38	646 ± 138	0.65 ± 0.1
p (n=4)	0.18	0.818	0.068
CTR	420 ± 56	599 ± 134	0.58 ± 0.06
TTX	540 ± 102	560 ± 134	0.74 ± 0.06
p (n=5)	0.1	0.41	0.18

TTX (Table 1). These results indicate TTX sensitive sodium channels are not involved in the generation of the light response in A1 cells and are inconsistent with action potentials propagating inputs to the cell from beyond the dendritic field via the axons.

Calcium imaging of A1 axons and dendrites

We used two-photon imaging to directly measure light-evoked calcium changes in the axons and dendrites of A1 cells. Two-photon imaging allows the excitation of fluorophores in the retina with minimal excitation of photoreceptors because the excitation source is an infrared laser and two-photon excitation of the fluorophore is restricted to the laser's focal point (Denk and Detwiler, 1999; Euler et al., 2002). Cells were filled with the calcium sensitive dye OGB-1 through the recording electrode (Figs 7A, 12A). We could unambiguously identify processes as axons by their small

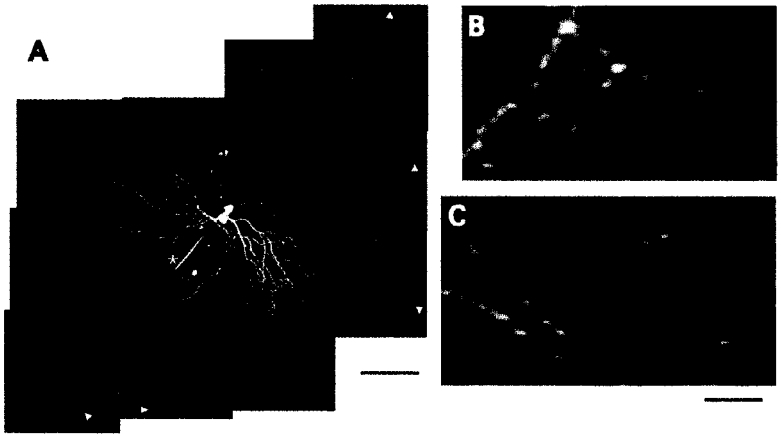

Fig 12: Oregon green filled A1 cell
A: An A1 amacrine cell filled with the calcium sensitive dye Oregon Green Bapta-1, and imaged on a two-photon microscope. The image is a reconstruction from several higher magnification images, each of which were compressions of image stacks in the z dimension. Thin axons are clearly seen extending beyond the restricted dendritic field (arrowheads). The recording electrode is marked with an asterisk. Scale bar = 100 μm. **B:** High magnification view of A1 dendrites. The dendrites are thick, moderately branched, and have spine-like protrusions. Scale bar = 20 μm. **C:** High magnification view of A1 axons. The axons are thin, sparsely branched and have bouton-like swellings. Scale bar = 20 μm.

diameter, lack of spines, sparse branching and extension greater than 500 μm from the soma (Fig 12C). Dendrites, conversely, were thicker, had spines, branched extensively and did not extend long distances from the soma (Fig 12B). Seven cells were filled with OGB. Five of those were filled sufficiently to image axons. We observed light-induced fluorescence changes in each of 7 axonal locations from those 5 cells. The dendritic calcium change was variable. Two of 7 cells had no light-induced fluorescence changes at any dendritic location imaged. The remaining 5 cells had light-induced fluorescence changes at all dendritic locations imaged except one (Fig 13D, location 2). In axonal and dendritic locations fluorescence changes occurred at light onset and offset, coincident with light induced depolarizations (Fig 13C). We then tested the effect of TTX

Figure 13: Calcium imaging in A1 axons and dendrites
A: An A1 cell filled with OGB-1 imaged with a two-photon microscope. The image is a reconstruction from several higher magnification images, each of which were compressions of image stacks in the z dimension. The axonal arbor was not completely filled, and the axons are very thin and dim, but several were traced as far as 600 μm from the soma. Scale bar = 100 μm. **B:** A tracing of the cell in A. The filled axons have arrowheads. The red numbered boxes indicate locations of linescans in figure D. Location 4 is beyond the scale of the image, 608 μm from the soma. **C:** Simultaneous electrical (blue) and optical (black) recording from an A1 cell showing the response to a 1s flash of a red LED (stimulus bar below traces) The vertical scale bar represents 15 mV and 20% fluorescence change (ΔF/F) (This recording was from the cell pictured in Fig 1A). **D:** Linescans from locations in B in response to a 1s red LED flash (stimulus bar at bottom) in the absence (black) and presence (red) of 0.5 μM TTX. The top 3 traces are from dendrites, and the bottom two axons. In location 3 a dendrite and axon were imaged simultaneously. Location 4 was beyond the scale of the image in B, 608 μm from the soma. The dendritic locations showed variable light induced fluorescence changes (location 2 had no change) and variable effect of TTX (location 1 was much more affected than location 3). The axonal fluorescence changes were always present and always completely abolished by TTX. Vertical scale bars represent 10% ΔF/F.

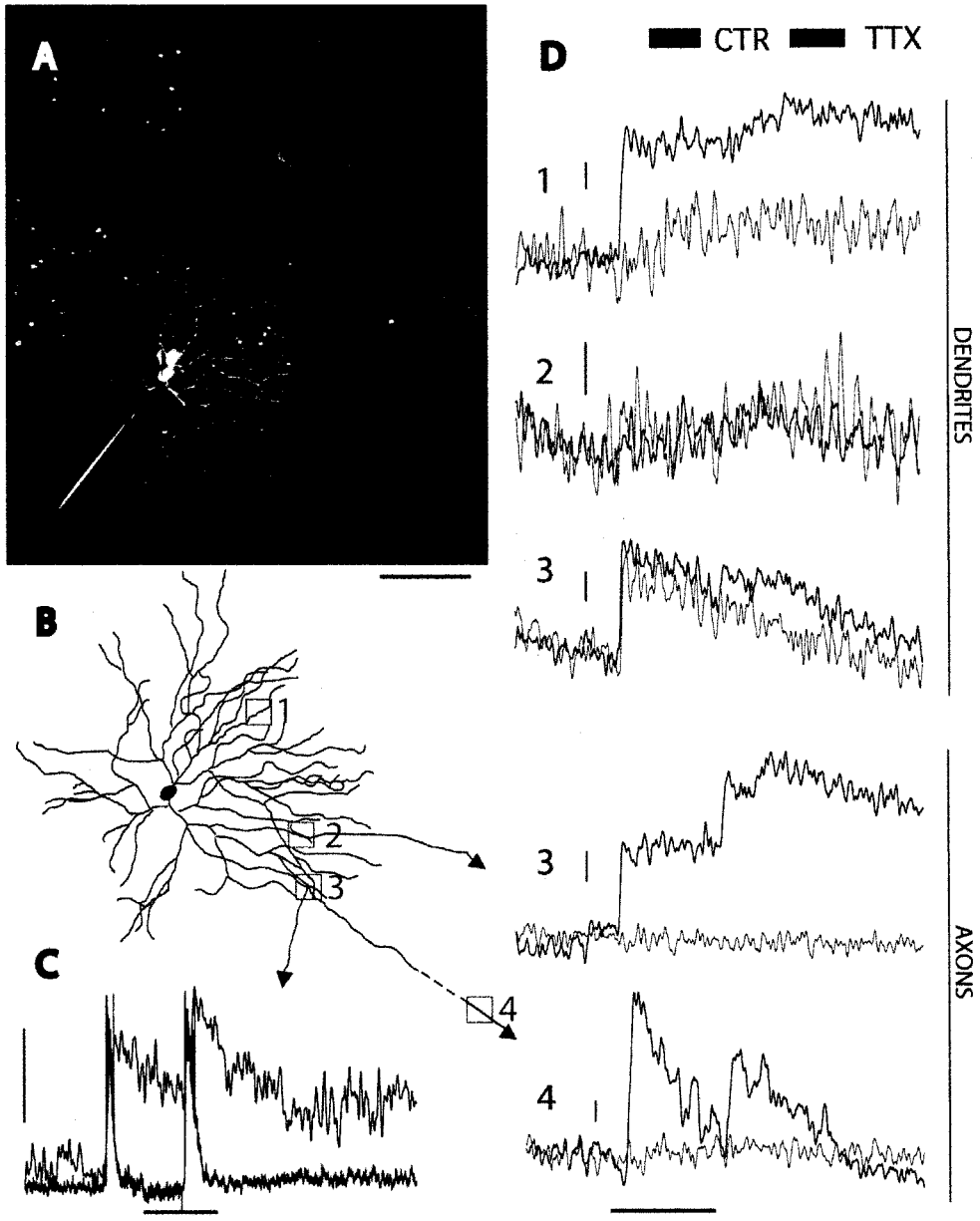
A
B
C
D
CTR
TTX
1
2
3
4
DENDRITES
AXONS

application on calcium transients in both dendrites and axons. If the dendrites are input structures and the axons output structures, with action potentials propagating along the axons, the calcium change observed in the axons should be blocked by TTX, which blocks action potentials. The calcium change in the dendrites, if independent of action potential propagation, should persist in the presence of TTX. After application of TTX, the calcium change in the axon was completely abolished in all cases (fluorescence change in TTX was 0.00 ± 0.019 of control, n=7 locations from 5 cells). By contrast the effect of TTX on dendrites was variable. In some cases there was little effect (Fig 13D, location 3), in some cases there was a more substantial effect (Fig 13D location 1). In the presence of TTX, the dendritic fluorescence change was decreased to 0.34 ± 0.09 (n=9 locations from 5 cells) of control, but not abolished. These results suggest that action potentials are required for an axonal but not dendritic calcium change.

Discussion

We have shown that A1 cells have antagonistic center-surround receptive field organization in both the ON and OFF fields. A1 surrounds are larger than those of ganglion cells but TTX does not affect the basic center-surround receptive field structure, so we conclude that action potentials do not contribute to the A1 center or large surround. We have also shown that TTX abolishes a light-induced calcium transient in A1 axons, but not in dendrites. Together, we interpret these results as supporting the hypothesis that A1 action potentials are generated in proximal axons and propagate away from the soma across the retina.

Receptive Field Organization

Our results are largely consistent with the A1 amacrine cell building its center-surround receptive field by combining inputs fron ON bipolar cells with OFF surrounds and OFF bipolar cells with ON surrounds. Consistent with this interpretation, primate diffuse bipolar cells have center-surround receptive fields (Dacey et al., 2000a). Our results with L-AP4, however, are inconsistent with a complete separation of the ON and OFF pathways. L-AP4 does not block OFF surround responses in A1 cells, which would be expected if they originated in the ON bipolar cell pathway. This could reflect the influence of electric coupling to neighboring A1 cells, whose OFF center responses are not blocked by L-AP4. The Gaussian receptive field surround diameters (the diameter at which a Gaussian receptive field fit decreases to 1/e of its maximum) of diffuse cone bipolar cells in peripheral primate retina are ~ 750 μm. Parasol ganglion cells, which have dendritic field sizes similar to the A1 cell and are thought to inherit their surrounds from bipolar cell input (McMahon et al., 2004), have Gaussian surround diameters similar to those of diffuse bipolar cells (Croner & Kaplan, 1995). As a comparison the A1 annulus response decreases to 1/e of its maximum at ~ 925 μm. The larger surround of A1 cells is inconsistent with its surround being generated purely from bipolar cell input. Coupling could also play a role in generating the large surrounds of A1 cells.

The A1 cell's antagonistic surround extends beyond its dendritic arbor. Surround responses could arise from input to the axonal arbor but several pieces of evidence argue against this. The amplitude of responses outside the dendritic arbor decreases to 50% within 760 μm. This surround size is slightly larger than a typical ganglion cell's surround but much smaller than the A1 axonal arbor. Responses from beyond the

dendritic arbor are unchanged after application of TTX. This suggests that action potentials propagating along the axons are not involved in inputs originating outside the dendritic arbor. If the antagonistic surround was generated by inhibitory GABAergic input to the axons, PTX would block the surround, but it does not. Together, these results are consistent with an axon-independent surround mechanism.

Parasol ganglion cell surrounds are thought to be generated in the outer retina by GABA independent horizontal cell feedback because surround antagonism is insensitive to PTX and TTX, which should affect inner retinal mechanisms of lateral inhibition (McMahon et al., 2004). Surround antagonism in A1 amacrine cells is not significantly changed in the presence of both PTX and TTX, suggesting that like parasol cell, an outer retinal mechanism involving horizontal cell feedback is primarily responsible for generating the antagonistic surround. Further pharmacological experiments examining the effect of drugs thought to affect horizontal cell feedback, such as Co^{2+}, HEPES and carbenoxelone (Vigh and Witkovsky, 1999; Kamermans et al., 2001; Hirasawa and Kaneko, 2003; McMahon et al., 2004; Vessey et al., 2005b) will help resolve the specific contributions of outer retinal feedback to the A1 surround.

PTX does have a significant effect on the light responses of A1 cells, substantially increasing their amplitude. GABAergic inhibition thus appears to have a role in A1 circuitry independent of surround antagonism. PTX would block any direct GABAergic inputs to A1 cells, but would also disinhibit other cells that receive GABAergic inhibition and that could interact with the A1 cell, for example glycinergic amacrine cells.

Light evoked calcium transients

The calcium response in A1 axons is completely abolished by TTX, indicating a necessity of voltage-gated sodium channels. We interpret this as meaning the action potentials recorded in the soma of A1 cells propagate along the axons. The observed calcium influx is probably due to the opening of voltage gated calcium channels caused by action potential propagation and depolarization. The A1 axons have swellings along their length that resemble presynaptic boutons. If these are in fact presynaptic structures, the presence of voltage gated calcium channels could serve to couple depolarization to vesicular neurotransmitter release. We also observe calcium changes in non-swelling locations. It is possible that there are presynaptic structures throughout the axons, or that calcium channels are present throughout the axons, independently of other presynaptic elements. Calcium increases in response to action potentials have been observed in myelinated axons of rat and mouse optic nerve (Lev-Ram and Grinvald, 1987; Zhang et al., 2006) but not in the unmyelinated intra-retinal portion of mouse ganglion cell axons (unpublished observation, DJ Margolis, AJ Gartland and PB Detwiler). Since there are no presynaptic elements in the myelinated axon, the action potential evoked calcium signals are thought to play a role in processes other than initiation of vesicular release, e.g. in coupling activity to energy metabolism (Zhang et al., 2006). This raises the possibility that the calcium increases in A1 axons participate in similar non-synaptic events in addition to or instead of playing a role in synaptic output.

The dendritic calcium change is heterogeneous. There were locations at which we observe no light-induced calcium change. The variability of the light-induced calcium increase at a specific dendritic location could be due to a number of factors, including the

proximity to synaptic inputs, the local distribution and concentration of voltage gated calcium channels, the affect of action potential back propagation and the contribution of calcium release from internal stores. When we do observe a dendritic calcium change it is diminished but not abolished by TTX. This effect of TTX could be due to dendritic sodium channels providing some boosting of the postsynaptic depolarization (Oesch *et al.*, 2005) or it could be due to back-propagation of action potentials from the soma/axons. We favor the back-propagation explanation because TTX does not have a substantial effect on the sub-spike voltage responses recorded at the soma and thus voltage-gated sodium channels do not seem to play an important role in integrating or boosting synaptic inputs and generating those responses. There are also examples from other cell types of a similar abatement of dendritic calcium increases after TTX application (Goldberg et al., 2003; Oesch et al., 2005) attributable to action potential back-propagation. In the context of action potential back-propagation, the variable effect of TTX on the dendritic calcium transients could be due to a variability of locations imaged relative to axonal origins where spikes are presumably initiated. We did not observe a dependence on distance from the soma of dendritic calcium changes (data not shown), but a more thorough and systematic sampling of dendritic tree locations will be needed to address this possibility.

Comparison to Previous Studies

A1 cell receptive field sizes previously reported were slightly larger than what we report here, and were on average ~1.5 times the dendritic field size (Stafford and Dacey, 1997). This can be reconciled with our results in that the large receptive fields probably

reflect the surround generating ON-OFF responses that are not readily distinguishable from center responses, as measured with small spot and bar stimuli not ideal for studying center-surround interactions. Volgyi et al. (Volgyi et al., 2001) studied the receptive field properties of six classes of polyaxonal amacrine cells in rabbit retina. They also found a correspondence of dendritic and receptive field sizes. Their PA1 cell, which they thought most analogous to the primate A1 cell, has a weakly inhibitory surround as measured by peak response amplitudes. This is in agreement with the A1 surround having an effect primarily on the area of the response, not the peak voltage. Receptive fields larger than dendritic fields have been used as an argument that axons could be providing input to axon-bearing amacrine cells (Freed et al., 1996). This may be a misinterpretation based on a failure to appreciate the influence of the surround.

Bloomfield (Bloomfield, 1996) found that TTX had no effect on the receptive field size of rabbit amacrine cells with dendritic fields less than 525 μm but that it decreased receptive field size in cells with larger dendritic fields, suggesting that action potentials were required to propagate information across large dendritic arbors. He also found good agreement between amacrine dendritic and receptive fields. Primate A1 amacrines have dendritic fields mostly smaller than 525 μm, and both the relation of dendritic to receptive field size, and the minimal effect of TTX on receptive field size are in agreement with Bloomfield's results.

A1 cell circuitry

Our study provides insight into the light response properties of A1 amacrine cells and provides new evidence that the axons function as spiking output structures. It will be

important in future work to determine the synaptic targets of the A1 cells and whether the dendrites are postsynaptic and axons presynaptic as the physiology predicts. Primate magnocellular-pathway ganglion cells have recently been shown to be influenced by stimuli outside their classical receptive field (Solomon et al., 2006). Another possible target for the A1 is an ON-OFF 'broad thorny' ganglion cell type that co-stratifies with the A1 dendritic and axonal fields in the middle of the IPL, has an ON-OFF transient light response and projects to the LGN and superior colliculus (Dacey et al., 2003). It is likely that the A1 cells are GABAergic (Mariani et al., 1987). If the A1 cell axons selectively contact the broad thorny cell it could provide long range inhibition from beyond the ganglion cells receptive field. This hypothesis could be explored by determining the degree to which the broad thorny cell, as well as other ganglion cell types in macaque retina, is strongly inhibited by global motion outside its receptive field.

The initial description of the A1 amacrine cell (Dacey, 1989) led to the postulate that the extensive network of axons operated as a unit, performing a global retinal function. More recent studies (Olveczky et al., 2003; Roska and Werblin, 2003) have provided some evidence that they are involved in inhibition in response to global image motion. Our results strengthen the overall hypothesis that the macaque A1 cell axons are spiking output structures and may serve as key elements for long-range lateral inhibition in the retina.

Chapter 2: Surround Generation and Horizontal Cell Feedback

Introduction

A basic characteristic of many neurons in the early visual system is a center-surround receptive field, whereby cells respond strongly to small stimuli but weakly to large stimuli (Kuffler, 1953). The center-surround receptive field first appears in cone photoreceptors (Verweij et al., 2003) and is thought to be generated by an inhibitory feedback signal from second order interneurons, the horizontal cells. Despite considerable study, the synaptic mechanism that mediates this feedback has been difficult to identify. Early experiments in goldfish retina suggested that horizontal cell feedback was mediated by a GABAergic synapse between horizontal cells and cones, however feedback is not affected by pharmacological manipulation of GABAergic neurotransmission (Kamermans and Spekreijse, 1999). It is currently thought that horizontal cell feedback operates via a non-vesicular mechanism that shifts the voltage activation curve of calcium channels on cone axon terminals to more negative potentials (Verweij et al., 1996). This shift opens calcium channels, causing a depolarization that opposes the light-induced photoreceptor hyperpolarization. Recent pharmacological results in goldfish have supported two different models of horizontal cell modulation of cone calcium channels. Sensitivity to carbenoxolone, which blocks gap junctions, has been used as evidence for an ephaptic mechanism of horizontal cell feedback to cones in which horizontal cell voltage changes cause current flow through hemichannel junctions on horizontal cell dendrites that modulates the extracellular voltage of the cone synaptic cleft to influence cone calcium channels (Byzov and Shura-Bura, 1986; Kamermans et al., 2001; Kamermans and Fahrenfort, 2004). Sensitivity to pH buffers, such as HEPES,

has been used as evidence for an alternative proton dependent mechanism, whereby horizontal cell voltage changes modulate the extracellular pH in the cone synaptic cleft to affect cone calcium channels (Barnes and Bui, 1991; Barnes, 2003; Hirasawa and Kaneko, 2003).

Pharmacological results using carbenoxolone in primate retina are consistent with these results from goldfish. The slow depolarization of the horizontal cell light response and the antagonistic surrounds of parasol ganglion cells and cones, which are all thought to be generated by horizontal cell feedback, are sensitive to carbenoxelone (Verweij et al., 2003; McMahon et al., 2004; Packer and Dacey, 2005). Exogenous pH buffers have not yet been tested on horizontal cell feedback to cones in primate retina, or on antagonistic surrounds of ganglion cells in any species.

Here, we examine the effect of HEPES and other pH buffers on measures of horizontal cell feedback to cones in primate parasol ganglion cells and horizontal cells. Our results confirm in mammalian retina that pH buffering attenuates measures of horizontal cell feedback, and are consistent with horizontal cell feedback operating via a process dependent on pH changes in the outer retina.

Methods

Tissue Preparation

Tissue was prepared as previously described (Dacey et al., 2000b). In brief, under deep barbituate anaesthesia, *Macaca nemestrina* or *fascicularis* retinas were enucleated and hemisected to remove the anterior pole including the lens and vitreous humor. The retina, choroid and pigment epithelium were dissected as a unit from the sclera. Radial

cuts were made to flatten the retina and it was fixed to a recording chamber with poly-L-lysine, vitreal side up. The chamber was mounted in an upright microsope. The retina was superfused with oxygenated Ames medium and maintained at 36 °C. The pH of the Ames was adjusted to 7.4 at RT (~ 21 °C), while bubbling with 95% O2/5% CO2. Ames was supplemented with additional pH buffers HEPES, MES, MOPS, PIPES and Tris adjusted to pH 7.4 under the same conditions. All buffers were obtained from Sigma (St Louis, MO). Buffering capacity was calculated as $2.3K_a[H^+][Buffer]/(K_a+[H^+])^2$ (Chesler, 1998) at our experimental pH of 7.4.

Electrical Recording

Glass microelectrodes (R = 250-500 MΩ) were filled with 2% Neurobiotin and 2% pyranine in 1M KCl. Retinas were stained with the vital dye acridine orange (several drops of 50 μM solution were added to the bath) or 10 μM of the nuclear dye DAPI (perfused over the retina for 30-60 min) and the retina and electrode were simultaneously visualized under fluorescence episcopic illumination. Parasol ganglion cell bodies were targeted based upon acridine orange staining of their large somas located in the ganglion cell layer. Horizontal cells were identified by DAPI staining of their nuclei, located at the outer edge of the outer nuclear layer and their distinctive spatial arrangement. Identity of cell types was confirmed after iontophoresis of pyranine allowed the examination of dendritic morphology in vitro. The electrode tip was positioned next to the soma and penetration was achieved by administering brief, high frequency current oscillations via the amplifier's buzz feature. Intracellular voltage was amplified (Axoprobe 2B, Axon

Instruments, Sunnyvale, CA) and digitized at 10 KHz. Data acquisition was controlled by custom software.

Visual Stimuli

Visual stimuli were generated by a digital projector (VistaGRAPHX 2500, Christie Digital, Cypress, CA) controlled by custom software through a VSG3 stimulus generator (Cambridge Research Systems, England)(Packer et al., 2001). Stimuli were focused through a 4x objective onto the retina. The retinal area covered by the stimulus was 2.96 X 2.22 mm. Stimuli used for receptive field measurements were white spots and annuli centered over the cell's receptive field which were modulated in steps or sinusoidally above and below a mid-photopic background luminance (L_{BKG}, estimated photon flux = 3.4 X 10^5 photons/μm^2 /second) at 100% contrast (contrast = L_{MAX}-L_{BKG}/L_{BKG}) at 2.03 Hz. A small test flash was first used to center the stimulus over the receptive field by manually moving it to elicit a maximum response. Twelve cycles of sinusoidal stimuli were presented to the cell and the responses were averaged and quantified by taking the amplitude of the fourrier component of the voltage response at the stimulus frequency. Statistical significance was determined by performing a Student's T-test, with a p value of less than 0.05 indicating significance.

Results

We first measured the antagonistic surround of parasol ganglion cells and then measured the slow depolarization of the horizontal cell light response, both of which are

thought to be mediated by horizontal cell feedback to cones. We examined the effect of exogenous pH buffering on both.

Parasol Cells

We recorded from 6 ON and 4 OFF parasol cells. There was no difference, other than the opposite phase of their responses, in their receptive field properties so they were treated as one group. We first measured center surround antagonism by presenting the cells with spots of increasing size. Figure 14A shows an example of a typical ON parasol cell response. A spot 300 μm in diameter, stimulating the receptive field center, evoked a robust, sustained response at light onset and a hyperpolarization at light offset. A spot 2000 μm in diameter, stimulating both the center and the surround, evoked diminished and more transient responses at light onset and transient hyperpolarizations at light offset, indicative of surround antagonism (Fig 14B). Figure 14C shows a plot of normalized response amplitude as a function of spot size of sinusoidally modulated spots. The response reaches a maximum at 300 μm and decreases at larger spot sizes. A 2000 μm spot evoked a response 0.32 ± 0.05 of maximum (n=10). In the presence of 20 mM HEPES, a 300 μm spot evoked a robust and sustained response (fig 14A, 16A) that was similar to control in amplitude (HEPES/control response amplitude = 1.32 ± 0.17, p = 0.13, n=10). The hyperpolarization at light offset is reduced compared to control. In response to a 2000 μm spot, cells also responded strongly and sustainedly in the presence of HEPES, unlike control (Fig 14B), indicating an attenuation of surround antagonism. As a function of spot size, the normalized response in the presence of HEPES is identical

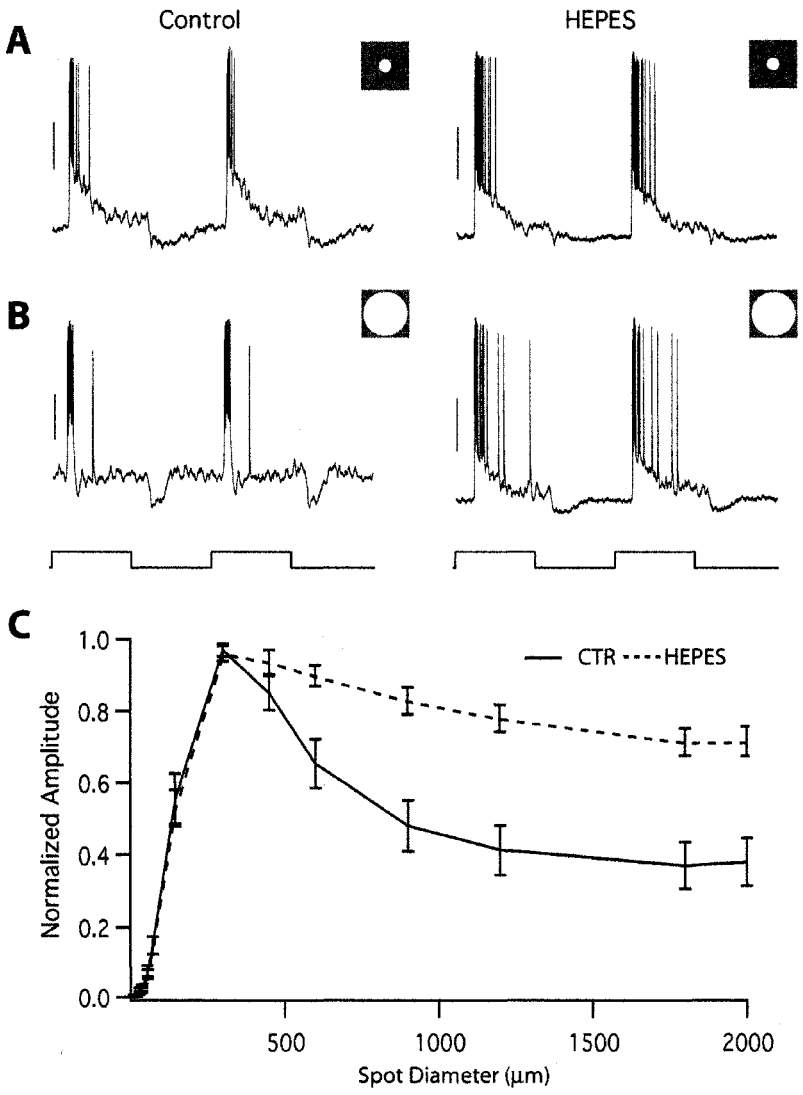

Figure 14: HEPES attenuates parasol ganglion cell surround: spots.
A: Responses of an ON parasol ganglion cell to a 300 µm diameter spot (stimulus trace below) flashed on and off at 250 ms intervals in the absence (left) and presence (right) of 20 mM HEPES. The responses are similar in both conditions. **B:** Responses of a parasol ganglion cell to a 2000 µm diameter spot (stimulus trace below) flashed on and off at 250 ms intervals in the absence (left) and presence (right) of HEPES. The control response is small and transient due to surround antagonism. The response in HEPES is larger and more sustained, indicating diminished surround antagonism. **C:** Response amplitude as a function of spot diameter in the absence (solid line) and presence (dashed line) of 20 mM HEPES. Stimuli were spots sinusoidally modulated at 2.03 Hz. Response amplitude was measured as the strength of the Fourier component of the membrane voltage at the stimulus frequency, normalized to the maximum amplitude. The responses at small spot diameters are similar, but the responses at larger spot diameters are larger in the presence of HEPES. n=10. Scale bars = 10 mV.

to control for spot sizes up to 300 μm, but is stronger at larger spot sizes (Fig 14C). In the presence of HEPES a 2000 μm spot evoked a response 0.72 ± 0.04 of maximum ($p < 0.001$ vs. control, n=10).

To study the surround in isolation we presented parasol cells with annuli with fixed outer diameters and increasing inner diameters. As in figure 14B, the response to a large spot is small and transient (Fig 15A). In response to an annulus, which minimally stimulates the center, the surround generates a response of opposite polarity to the center with a strong, sustained depolarization at light offset and hyperpolarization at light onset (Fig 15B, compare to Fig 14A). Figure 15C shows a plot of normalized response amplitude as a function of annulus inner diameter (the outer diameter was fixed at 2000 μm) in response to sinusoidally modulated annuli. The response is small at small inner diameter annuli, reaches a maximum at 300 μm and then decreases. In the presence of HEPES cells responded more strongly than control to small inner diameter annuli due to diminished center-surround antagonism (Fig 15A). In response to larger inner diameter annuli the response is smaller than control, with transient responses at light onset and offset. This is consistent with a weakened surround producing a smaller, more transient OFF response, and the center, the edge of which is stimulated by the annulus and which is not antagonized as strongly by the weak surround, producing a small ON response (Fig 15B, C, 16B). The response to a 300 μm inner diameter annulus was decreased to 0.38 ± 0.1 of control ($p < 0.001$, n=10).

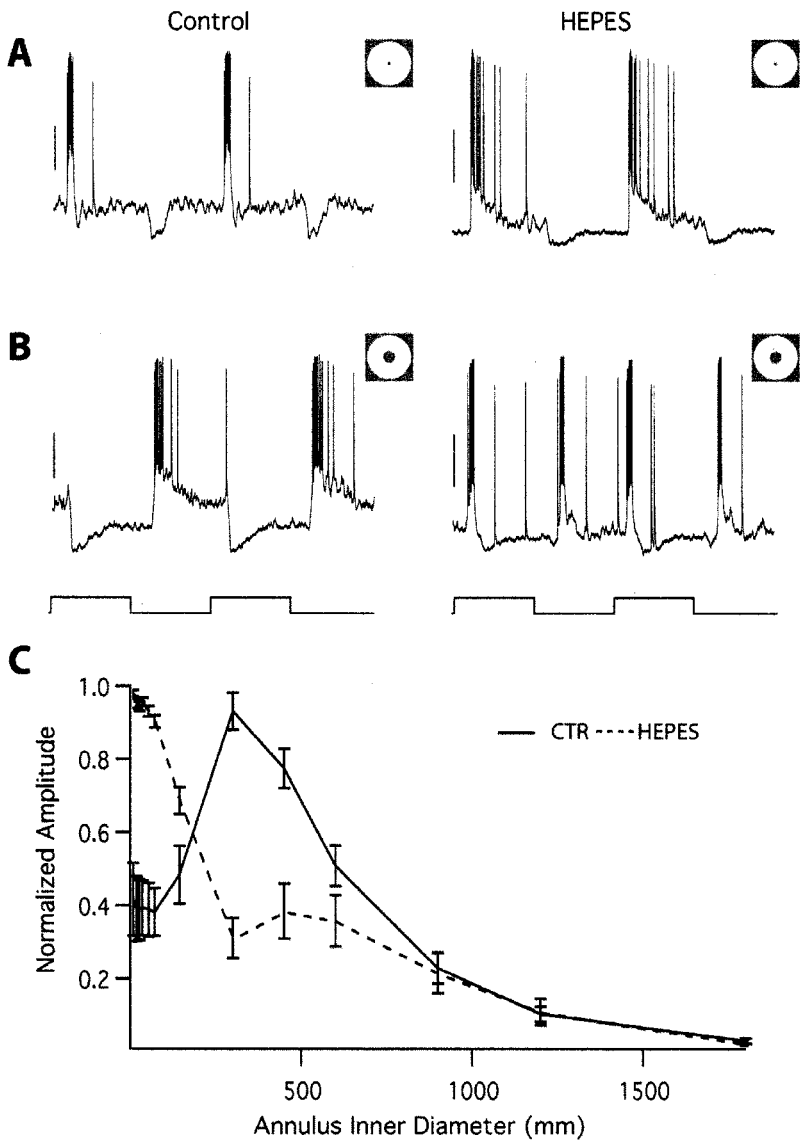

Figure 15: HEPES attenuates parasol ganglion cell surround: annuli.
A: Responses of an ON parasol ganglion cell to a 2000 μm diameter spot (stimulus trace below) flashed on and off at 250 ms intervals in the absence (left) and presence (right) of HEPES. The response in the presence of HEPES is larger, indicating diminished surround antagonism. **B**: Responses of a parasol ganglion cell to an annulus with 2000 μm outer diameter and 450 μm inner diameter flashed on and off at 250 ms intervals (stimulus trace below) in the absence (left) and presence (right) of 20 mM HEPES. The response in the presence of HEPES is diminished, indicating decreased surround strength. **C:** Response amplitude as a function of annulus inner diameter (outer diameter is 2000 μm) in the absence (solid line) and presence (dashed line) of 20 mM HEPES. Stimuli were spots sinusoidally modulated at 2.03 Hz. Response amplitude was measured as in Figure 1. The responses at small annulus inner diameters are larger, and the responses at larger annulus inner diameters are smaller in the presence of HEPES. n = 10. Scale bars = 10 mV

Figure 16 shows cumulative data of the effect of HEPES on parasol ganglion cells. Receptive field center responses to 300 μm soinsoidally modulated spots were not significantly different in amplitude in the presence of HEPES (fig 16A). The surround response to annuli with 300 μm inner diameter and 2000 μm outer diameter modulated sinusoidally were significantly smaller in amplitude in the presence of HEPES (fig 16B). Surround antagonism, measured as the fraction of the maximum spot response evoked by a 2000 μm spot also was significantly diminished in the presence of HEPES (fig 16C).

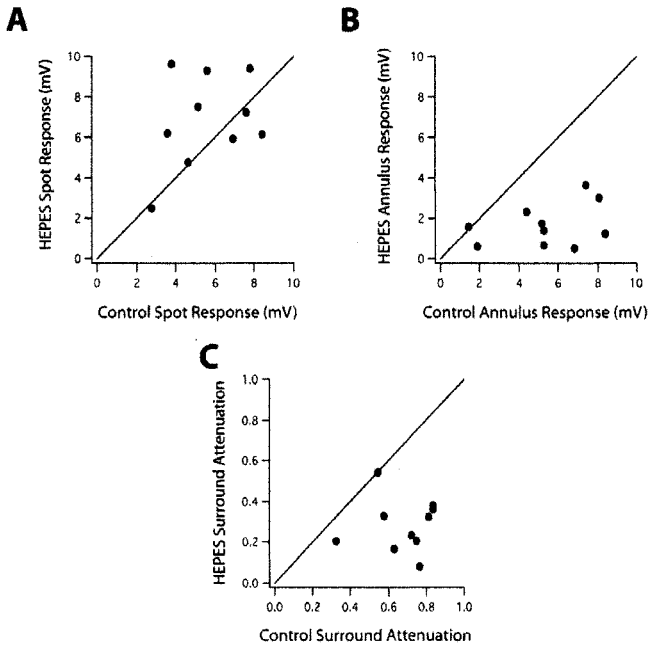

Figure 16: HEPES attenuates parasol ganglion cell surround: cumulative data.
A: Amplitudes of the responses to sinusoidally modulated 300 μm spots in the presence of HEPES plotted against control responses. n=10. The responses are not significantly different in the presence of HEPES. **B:** Amplitude of the responses to sinusoidally modulated 300 μm inner diameter, 2000 μm outer diameter annuli in the presence of HEPES plotted against control responses. n=10. The responses to annuli are significantly smaller in the presence of HEPES. **C:** Amplitude of surround antagonism, measured as the fraction of the maximal spot response that a 2000 μm spot evokes, in the presence of HEPES plotted against control surround antagonism. n=10. Surround antagonism is significantly attenuated in the presence of HEPES.

Horizontal Cells

At the onset of a light step, horizontal cells hyperpolarize rapidly followed by a slow depolarization to a new steady-state membrane potential. At the offset of a light step they respond oppositely with a rapid depolarization that overshoots the dark resting membrane potential a slow hyperpolarization back to the dark potential (fig 17A). The overshoot and slow hyperpolarization at light offset are not well understood, but the slow depolarization at light onset is likely due to horizontal cell feedback to cones because it is stronger in response to large stimuli than small stimuli, it is correlated with measures of horizontal cell feedback in cones themselves (Baylor et al., 1971; Stone and Witkovsky, 1987) and pharmacological agents which block feedback to cones and the surrounds of cones also block the slow depolarization (Kamermans et al., 2001; Verweij et al., 2003; Packer and Dacey, 2005).

Consistent with previous work, the amplitude of the slow depolarization increased with stimulus size (Fig 17B). Depolarization/hyperpolarization ratio was 1.5 ± 0.02 times greater in response to a 2000 μm spot than to a 144 μm spot (n=2), which is approximately the dendritic field size of peripheral H1 horizontal cells. The hyperpolarization amplitude and depolarization amplitude varied from cell to cell but the ratio of depolarization to hyperpolarization was near constant at a given spot size. In response to a 2000 μm spot, which was used in all subsequent experiments, depol./hyperpol. = 0.27 ± 0.01 (n=25) (fig 17B). We therefore quantified the depolarization by normalizing to the hyperpolarization.

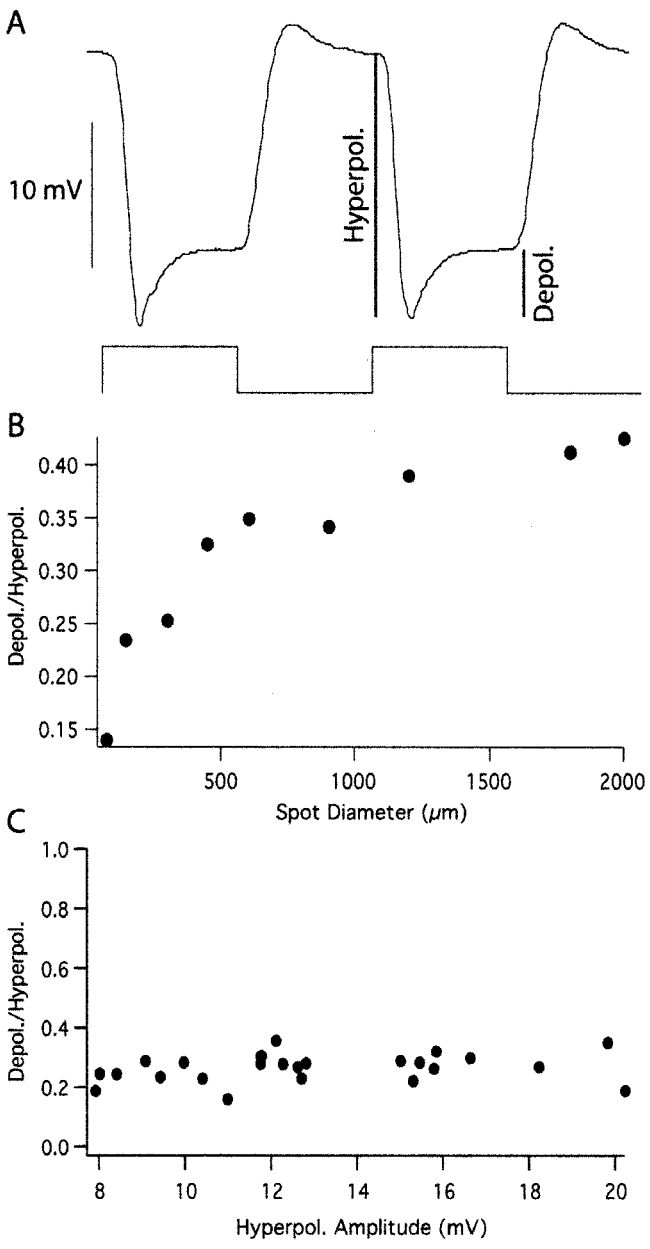

Figure 17: Horizontal cell light response.
A: Response of a horizontal cell to a 2000 μm spot flashed on and off at 250 ms intervals (stimulus trace below). Scale bar = 10 mV. **B:** Ratio of depolarization amplitude to hyperpolarization amplitude as a function of spot diameter (from 72 μm to 2000 μm) for a single cell. The slow depolarization increases relative to the hyperpolarization as spot diameter increases. **C:** Ratio of depolarization to hyperpolarization amplitude (as shown in A) as a function of hyperpolarization amplitude in response to 2000 μm spots. n = 25. The ratio of depolarization to hyperpolarization is constant across all response amplitudes.

Figure 18: HEPES dose response.
A: Response of a horizontal cell to a 2000 μm spot flashed on and off at 250 ms intervals (stimulus trace below) at increasing concentrations of HEPES on the same scale (above) to show increased response amplitude, and normalized (below) to show decreased slow depolarization amplitude. Scale bars = 10 mV. **B:** Hyperpolarization amplitude as a function of [HEPES]. HEPES increases the hyperpolarization amplitude in a dose dependent manner. n = 3-5. **C:** Ratio of depoarization to hyperpolarization as a function of [HEPES]. HEPES decreases the depolarization in a dose dependent manner. n = 3-5.

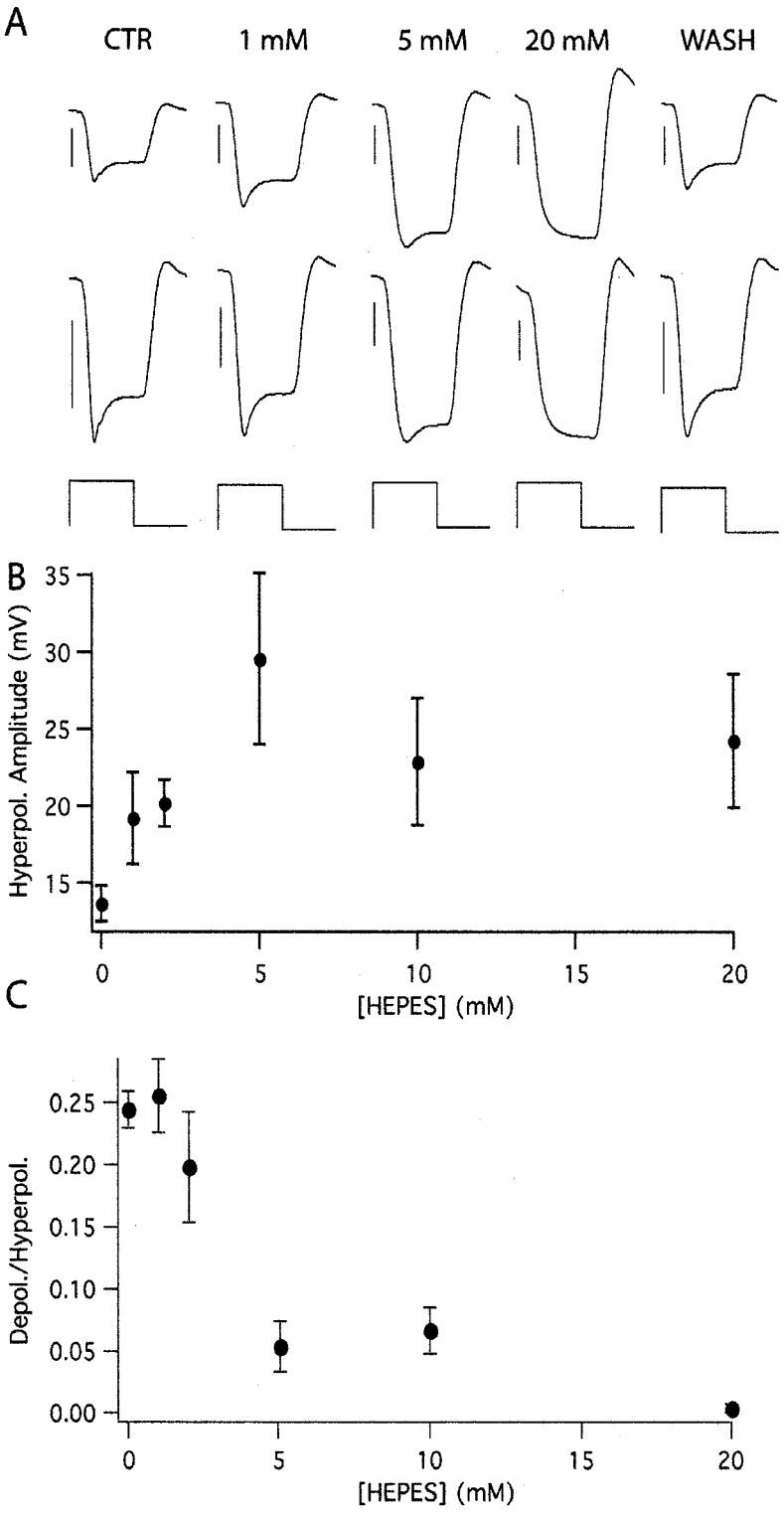
A
CTR
1 mM
5 mM
20 mM
WASH
B
Hyperpol. Amplitude (mV)
35
30
25
20
15
0
5
10
15
20
[HEPES] (mM)
C
Depol./Hyperpol.
0.25
0.20
0.15
0.10
0.05
0.00
0
5
10
15
20
[HEPES] (mM)

We examined the effect of the pH buffer HEPES on the horizontal cell light response (fig 18). At low concentrations HEPES had no significant effect on the hyperpolarization or depolarization amplitudes (depol./hyperpol. = 0.25 ± 0.01 in control, 0.26 ± 0.03 in 1 mM HEPES, n=4). At higher concentrations (5, 10 mM) HEPES significantly increased the hyperpolarization amplitude, and decreased the depolarization amplitude. 20 mM HEPES did not further increase hyperpolarization amplitude, but completely abolished the depolarization (depol./hyperpol. = 0.01 ± 0.01 in 20 mM HEPES, n=5). The effect of HEPES could be reversed by returning to control solution. HEPES did not significantly change the resting membrane potential of horizontal cells (CTR = -39.0 ± 3.3 mV, 20 mM HEPES = -45.6 ± 8.0 mV, p = 0.30, n=5). We used sucrose to produce an equivalent osmolality increase to 20 mM HEPES and observed no significant change in the slow depolarization (depol./hyperpol. = 0.29 ± 0.01 in control, 0.29 ± 0.01 in sucrose, p = 0.58, n=3).

To quantify further the effect of HEPES on the horizontal cell light response we measured the slope of the voltage response in the absence and presence of HEPES. The control response slope has an initial negative component corresponding with the initial steep hyperpolarization. The slope reaches a peak negative value, then becomes less negative as the hyperpolarization becomes less steep. The slope eventually returns to zero, the zero crossing corresponding to the peak hyperpolarization. The response then overshoots zero, corresponding with the initial steep depolarization, before returning to zero, when the voltage has reached its steady state (Fig 19A). We quantified the slope by taking the time at which it crosses 50 % of its peak negative value on its downward and upward phase (Fig 19B). The downward phase is not significantly affected by HEPES

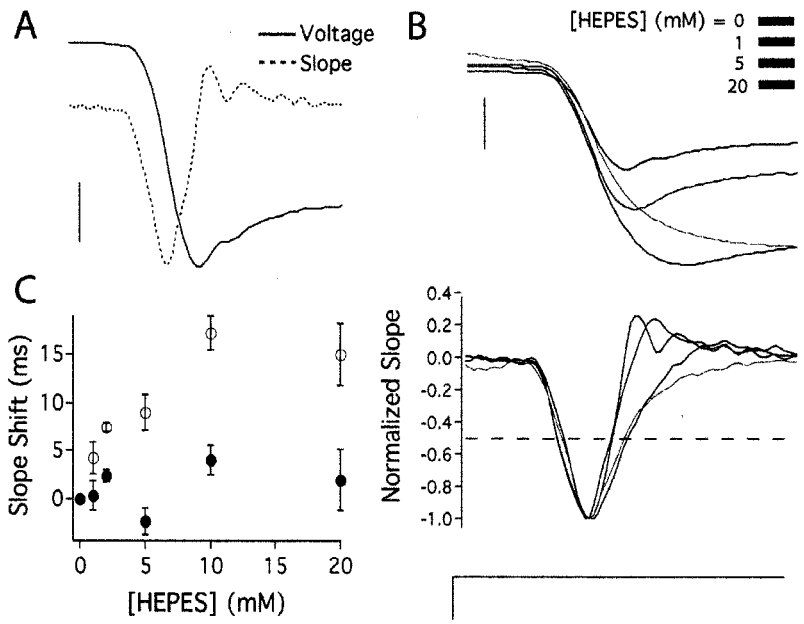

Figure 19: HEPES effect on the slope of the H1 response
A: Response of a horizontal cell to the onset of a 2000 μm spot (solid line) and the slope of the response (dotted line). Scale bar = 10 mV (voltage), 3 mV/ms (slope). **B:** Responses (above) and slope (below) of a horizontal cell to the onset of a 2000 μm spot at 0 (black), 1 (green), 5 (blue) and 20 (red) mM HEPES. **C:** Time of 50% slope crossing relative to control on the downward (filled circles) and upward (open circles) directions (see dotted line in B) as a function of [HEPES]. n = 3-5. HEPES shifts the upward crossing, but not the downward crossing.

(20 mM HEPES shifts the 50 % crossing time 1.9 ± 3 ms relative to control, p = 0.58, n=5), indicating the initial light response, presumably prior to the effect of feedback, is unaffected by HEPES. The upward 50% crossing is affected by HEPES in a dose-dependent manner, with 20 mM HEPES shifting this point by 15 ± 3 ms relative to control (p = 0.009, n=5). This suggests that HEPES only has an effect on later portions of the light response, once feedback has started to affect the light response.

Figure 20: Other buffers attenuate the slow depolarization.
A: Responses of horizontal cells to a 2000 μm spot flashed on and off at 250 ms intervals (stimulus trace below) at two concentrations of Tris (above) and MOPS (below). The control and 20 mM MOPS traces are from one cell, and the 5 mM MOPS trace is from a different cell. Both Tris and MOPS decrease the depolarization in a dose dependent manner. Scale bars = 10 mV. **B:** Ratio of depolarization to hyperpolarization as a function of buffer capacity for all buffers tested. The effect of all buffers on the depolarization is correlated with their buffering capacity. n=3-5 **C:** Ratio of depolarization to hyperpolarization at 5 mM Buffer as a function of buffer pKa. Buffers with pKas closer to our experimental pH had a stronger effect on the depolarization. n=3-5.

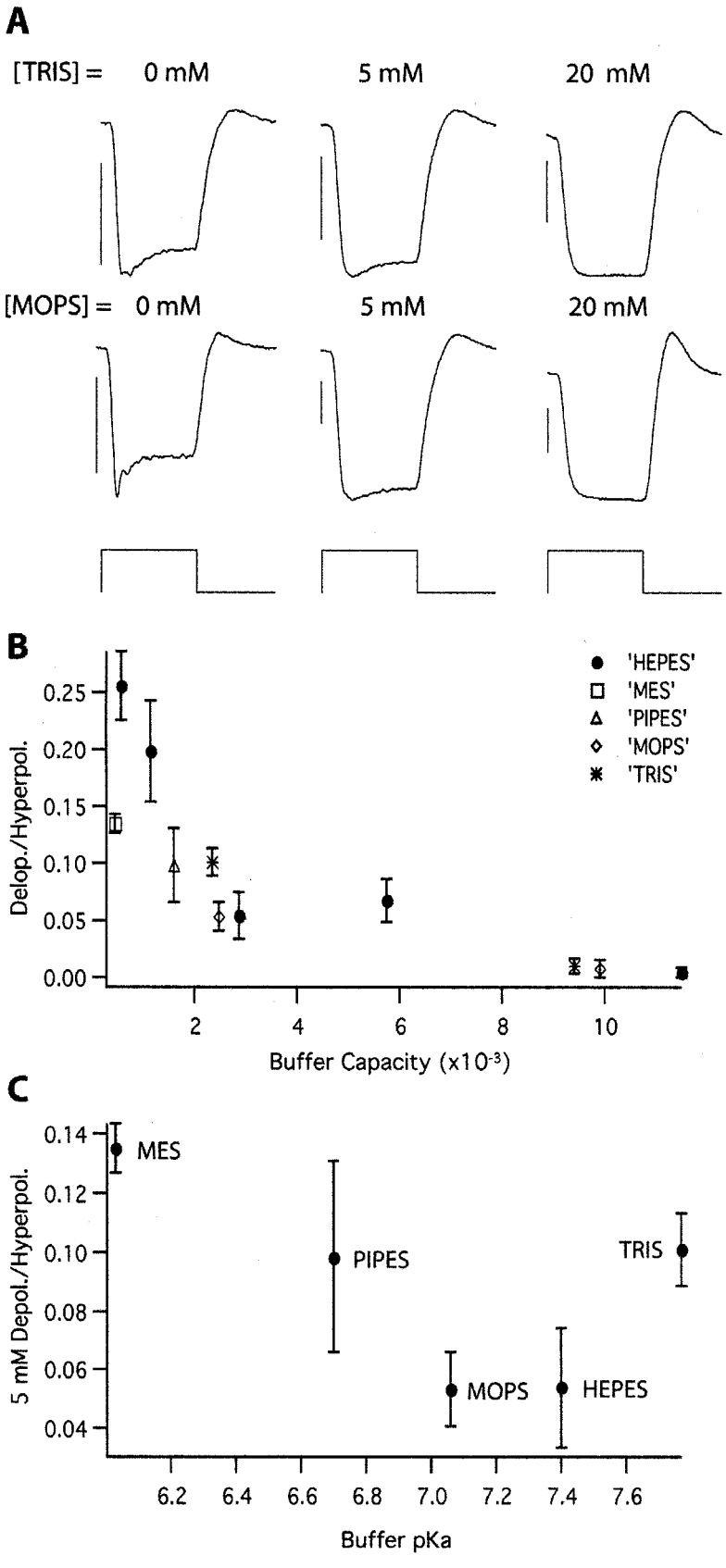
A
[TRIS] = 0 mM
5 mM
20 mM
[MOPS] = 0 mM
5 mM
20 mM
B
'HEPES'
'MES'
'PIPES'
'MOPS'
'TRIS'
Delop./Hyperpol.
0.25
0.20
0.15
0.10
0.05
0.00
2
4
6
8
10
Buffer Capacity (x10-3)
C
5 mM Depol./Hyperpol.
0.14
0.12
0.10
0.08
0.06
0.04
MES
PIPES
TRIS
MOPS
HEPES
6.2
6.4
6.6
6.8
7.0
7.2
7.4
7.6
Buffer pKa

To test for any non-specific action of HEPES, we examined the effect of several other pH buffers on the horizontal cell light response. We used other structurally similar "Good" buffers (Good et al., 1966) MOPS, PIPES and MES, which have an aminosulfonate moiety in common with HEPES but have different pKas, as well as the structurally different buffer Tris. Shown in figure 14, both MOPS and Tris diminished the horizontal cell slow depolarization in a concentration dependent manner. The effect of each exogenous buffer on the slow depolarization was correlated with their calculated buffering capacity (fig 20B). Additionally, we compared the effect of all buffers at 5 mM as a function of their pKa. The buffers with the strongest effect at 5 mM were those with pKas closer to the pH of our experiments (7.4), MOPS and HEPES. Buffers with pKas further away, most notably MES, had weaker effects (fig 20C). These experiments suggest that the effect of exogenous buffers is due to their pH buffering capacity, rather than non-specific effects.

We attempted to manipulate the normal bicarbonate buffering system of the extracellular solution by switching from normal 22 mM bicarbonate/5% CO_2 to 44 mM bicarbonate/10% CO_2, and adding exogenous carbonic anyhdrase (CA), which speeds the bicarbonate buffering system. There was no significant change in the depolarization in the presence of 44 mM bicabonate + 10 mg/L CA (depol./hyperpol. = 0.29 ± 0.01 in control, 0.32 ± 0.02 in 2X bicarbonate + CA, $p = 0.11$, $n=5$).

Pharmacological blockade of gap junctions has been shown to affect horizontal cell feedback and ganglion cell surrounds (Kamermans and Fahrenfort, 2004; McMahon et al., 2004). To test for any non-specific effect of HEPES on gap junctions we measured the spatial receptive fields of H1 horizontal cells. H1 cells have receptive fields much

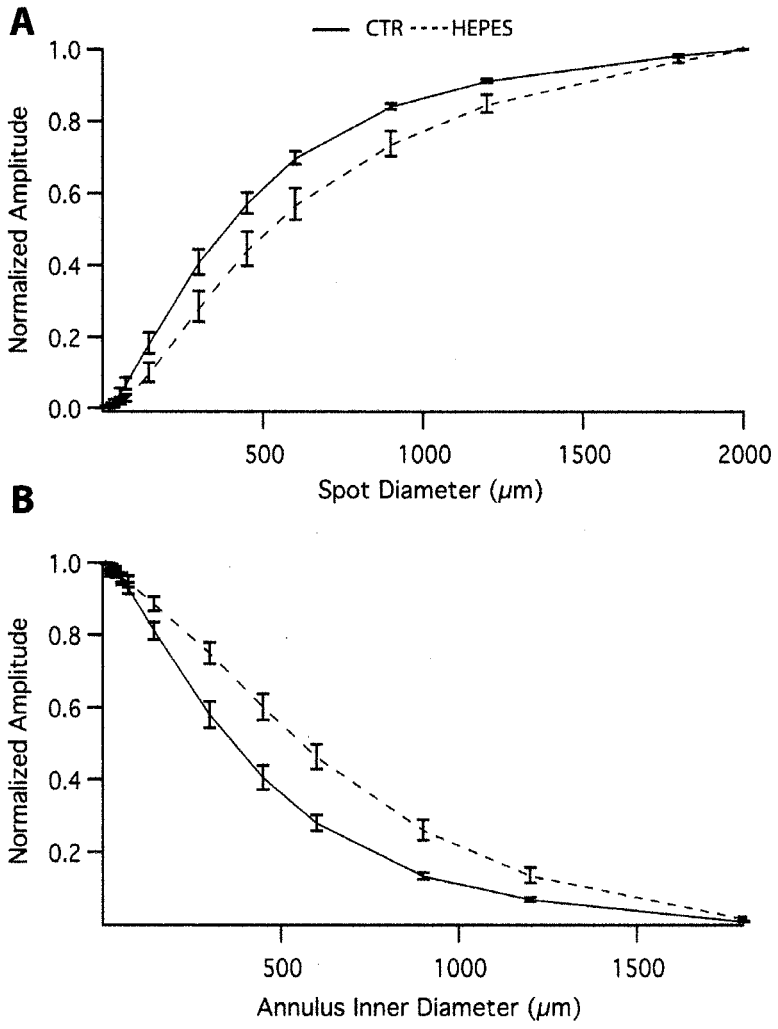

Figure 21: HEPES effect on H1 cell receptive field.
A: Horizontal cell response as a function of spot diameter in the absence (solid line) and presence (dashed line) of HEPES. Stimuli were spots sinusoidally modulated at 2.03 Hz. Response amplitude was measured as the strength of the Fourier component of the membrane voltage at the stimulus frequency, normalized to the maximum amplitude. HEPES causes responses to plateau at larger spot sizes, indicating larger receptive field size. n=9. **B:** Horizontal cell response as a function of annulus inner diameter (outer diameter was fixed at 2000 μm) in the absence (solid line) and presence (dashed line) of 20 mM HEPES. Stimuli and measurement parameters were the same as in A. Responses are stronger at larger annulus inner diameters in the presence of HEPS indicating larger receptive field size. n=9.

larger than their dendritic fields, which are generated by coupling to other horizontal cells via gap junctions (Packer and Dacey, 2005). In response to sinusoidally modulated spots

of increasing diameter, H1 cells responded increasingly and eventually plateau (Fig 21A). As an arbitrary estimate of receptive field size we measured the spot diameter at which the response reached 90% of its maximum (1144 ± 27 μm). In the presence of HEPES, the response plateaus at larger spot sizes than control. The response reached 90% of its maximum at 1374 ± 91 μm, indicating an increase in receptive field size ($p = 0.037$, $n = 9$). We also measured the response to sinusoidally modulated annuli with increasing inner diameters. The response decreases as the annulus inner diameter increases (Fig 21B). As an arbitrary estimate of receptive field size we measured the point at which the annulus response function decreased to 10 % of its maximum (1043 ± 35 μm). In the presence of HEPES, cells responded more strongly at larger annulus inner diameters than in control, and decreased to 10% of their maximum at 1321 ± 66 μm. This also indicates an increase in receptive field size ($p = 0.001$, $n = 9$). Both of these measures indicate that gap junctional coupling between horizontal cells is not blocked by HEPES, and is if anything strengthened.

Discussion

HEPES blocks the surrounds of parasol ganglion cells and also blocks the horizontal cell slow depolarization in a dose dependent manner. Other pH buffers attenuate the horizontal cell slow depolarization in correlation with their relative pH buffering capacities. HEPES increases the receptive field size of H1 horizontal cells. Together these results suggest that HEPES and other pH buffers affect horizontal cell feedback via their pH buffering properties, and that feedback requires pH changes in the outer retina.

Parasol Cell Surrounds

In the presence of HEPES the surround response of parasol cells is weak and ON-OFF. In an ON parasol cell, for example, the weak OFF response is consistent with a weakened surround, and the weak ON response likely results from the anuulus inner edge stimulating the outer edge of the receptive field center, which is not fully antagonized by the weak surround.

Previous work in the primate retina has shown that carbenoxolone and cobalt, which interfere with horizontal cell feedback, attenuate parasol ganglion cell surrounds, while TTX, PTX and STR, which interfere with amacrine cell feedback, do not (McMahon *et al.*, 2004). That HEPES, which also interferes with horizontal cell feedback, attenuates the surrounds of parasol cells strengthens the connection between horizontal cell feedback in the outer retina and ganglion cell surrounds. Based on Gaussian receptive field fits, cobalt and carbenoxolone attenuated parasol ganglion cell surrounds by ~ 60%, which is approximately the same as the attenuation HEPES causes, consistent with them acting on the same feedback mechanism.

Horizontal cells

HEPES increased the light response amplitude and receptive field size of horizontal cells, consistent with a previous study (Hare and Owen, 1998) in which the normal bicarbonate buffer was replaced with HEPES. It was hypothesized that because HEPES cannot cross cell membranes, unlike bicarbonate, intracellular pH regulation was perturbed causing the observed changes in retinal physiology. In our experiments the

normal bicarbonate buffering system of the extracellular solution was augmented, not replaced, by HEPES. Bicarbonate is still present to cross cell membranes and participate in intracellular pH regulation so the effects of HEPES must be caused by the increased extracellular buffering capacity it provides. The increased horizontal cell response amplitude is at least partly attributable to a lack of feedback that would normally attenuate the response. Consistent with this interpretation, our measurements show that the slope of the initial component of the response, presumably prior to the effect of feedback, is unaffected by HEPES. The increased receptive field size could be due to better transmission of responses over the network of coupled horizontal cells due to the increased response amplitudes of all horizontal cells in the absence of feedback.

We used the slow depolarization of the horizontal cell light response as a measure of horizontal cell feedback to cones. The origin of the slow depolarization is not fully known but there is strong evidence that it is correlated with horizontal cell feedback to cones. It is much stronger in response to large spots than small spots (Baylor et al., 1971; Stone and Witkovsky, 1987), suggesting it is mediated by lateral horizontal cell feedback over large retinal areas. In responses to large spots, cones have a depolarizing inflection in their light response that is not present in responses to small spots. This inflection is coincident with the horizontal cell slow depolarization, and the temporal relationship of the two is consistent with horizontal cell feedback (Baylor et al., 1971). Pharmacological agents that block feedback invariably block the slow depolarization (Kamermans et al., 2001; Verweij et al., 2003; Packer and Dacey, 2005). Finally, models of outer retinal processing that include horizontal cell feedback reproduce the slow depolarization (Smith, 1995; Smith et al., 2001; van Hateren, 2005). HEPES has previously been shown

to affect horizontal cell modulation of cone calcium channels in non-mammalian retina (Hirasawa and Kaneko, 2003; Vessey et al., 2005a; Cadetti and Thoreson, 2006). Our results are consistent with these findings and are another example of a pharmacological manipulation that blocks horizontal cell feedback also blocking the horizontal cell slow depolarization, strengthening the link between the two.

Similar to HEPES, carbenoxolone and cobalt attenuate the slow depolarization of primate horizontal cells (Packer and Dacey, 2005). There is evidence that both carbenoxolone (Vessey et al., 2004) and cobalt (Vessey et al., 2005a) directly inhibit cone voltage gated calcium channels. In the context of the proton hypothesis of horizontal cell feedback to cones, carbenoxolone and cobalt could both inhibit the ability of horizontal cell feedback to modulate cone calcium channels by directly blocking those channels. Consistent with this interpretation, carbenoxelone and cobalt both hyperpolarize primate horizontal cells and decrease the amplitude of their light response (Packer and Dacey, 2005), which would be expected if the voltage gated calcium channels responsible for vesicular release were inhibited. In contrast, HEPES increased the amplitude of horizontal cell light responses and does not affect the horizontal cell resting potential, consistent with a block of the ability of horizontal cells to modulate calcium channels rather than a block of the channels themselves.

Doubling the concentration of bicarbonate buffer in the external solution did not have a significant effect on the horizontal cell light response both in the absence and presence of exogenous CA (data not shown), which speeds the bicarbonate buffering system. Several factors could account for this: It is possible that the retina's endogenous system of regulating bicarbonate buffering makes it more difficult to manipulate this

system experimentally. It is also possible that the bicarbonate buffering system simply does not operate effectively in the cone pedicle. CA staining is strong in the outer plexiform layer, but this staining is thought to be restricted to Müller glia (Nagelhus *et al.*, 2005; Ochrietor *et al.*, 2005), which do not extend processes into the synapse itself (Sarantis and Mobbs, 1992). The restricted nature of the synapse might also exclude exogenous CA, which is a large molecule (mw = 31 kD). In the absence of CA, the bicarbonate buffering system has an equilibration time constant of ~ 30 s (Voipio, 1998), and adding additional bicarbonate would not be expected to effectively buffer pH changes on the time scale of our measurements.

The main alternative to the pH hypothesis of horizontal cell feedback is the ephaptic hypothesis, whereby connexin hemichannels at horizontal cell dendritic tips allow current flow from horizontal cell dendrites to change the extracellular voltage in the synapse and modulate cone calcium channels (Kamermans et al., 2001; Kamermans and Fahrenfort, 2004). Several Good buffers including HEPES and MES have been shown to inhibit connexin channel activity directly, specifically channels containing connexin-26 (Bevans and Harris, 1999), which is thought to be the type constituting hemichannels in fish retina (Janssen-Bienhold et al., 2001). We believe that these buffers are not acting by blocking hemichannels for several reasons: Tris, which does not inhibit connexin channel activity, has a similar effect on the horizontal cell slow depolarization as HEPES, consistent with results from goldfish (Hirasawa and Kaneko, 2003). The action of all the buffers tested was correlated with their buffering capacity, rather than their absolute concentration. Finally, the gap junction-dependent receptive field of H1

horizontal cells was increased in size by HEPES, not decreased as would be expected if HEPES non-specifically blocked gap junctions.

We have shown that both the slow depolarization of the horizontal cell light response and the antagonistic surround of parasol ganglion cells are attenuated by exogenous pH buffers, strengthening the link between the horizontal cell slow depolarization, horizontal cell feedback to cones, and surround generation. In the primate retina to date, surround pharmacology is consistent in that agents that block surrounds of ganglion cells also block the horizontal cell slow depolarization and the surrounds of cones. It will be interesting in future experiments to examine the effect of pH buffers on the cone receptive field.

Chapter 3: Opponency in the small bistratified ganglion cell

Introduction

The nervous system generates our perception of all the colors in the visual world from the absorption of photons by only three cone types. It accomplishes this by comparing the output of cones in a process called opponency, in which downstream cells receive antagonistic inputs from different types of cones. In the primate visual system, there are neural pathways that compare the output of long (L) to middle (M) wavelength sensitive cones, and that compare the output of short (S) wavelength sensitive cones to both L and M cones. Cells that respond to the onset of a blue light and the offset of a yellow light were first identified in extracellular recordings in the lateral geniculate nucleus (LGN) (De Valois et al., 1958), where it was subsequently discovered that the blue ON and yellow OFF spatial receptive fields were coextensive (type II) as opposed to concentric center-surround (type I) (Wiesel and Hubel, 1966). The morphological retinal ganglion cell type that embodies the blue ON physiological type was identified as the small bistratified cell (Dacey, 1993; Dacey and Lee, 1994). The small bistratified cell has dendrites in both the inner, ON and outer, OFF sublayers of the inner plexiform layer. It was therefore proposed that the small bistratified cell generates blue-yellow opponency by receiving input to its inner dendrites from short wavelength sensitive ON bipolar cells and input to its outer dendrites from long wavelength sensitive OFF bipolar cells. This would create both the blue ON and yellow OFF light responses and the type II receptive field organization. Electron microscopic studies in the macaque fovea have shown that small bistratified cells inner dendrites are postsynaptic to bipolar cells connected to S

cones and outer dendrites are postsynaptic to bipolar cells connected to L and M cones (Calkins et al., 1998), consistent with this basic circuitry.

Here we pharmacologically test the hypothesis that blue-yellow opponency is generated by antagonistic ON and OFF pathway inputs to small bistratified cells. As expected, blockade of the ON pathway completely abolishes the S ON response but also significantly attenuates the yellow OFF response, suggesting it is generated predominantly by the ON pathway. The L-AP4 resistant yellow OFF response has its own center-surround receptive field structure. Blocking GABAergic and glycinergic inhibitory inputs does not affect the basic S ON or L+M OFF light responses, but the pH buffer HEPES selectively attenuates the L+M OFF response, suggesting horizontal cell feedback from L and M cones to S cones generates the L+M OFF response. We propose a model of small bistratified cell circuitry in which the yellow OFF opponent signal is generated by HII horizontal cell feedback from L and M cones to S cones in the outer retina as a conventional surround. The L+M OFF bipolar input modulates this receptive field, making it more type II-like (Fig 27).

Methods

Tissue Preparation

Tissue was prepared as previously described (Dacey et al., 2000b). In brief, under deep barbituate anaesthesia, *Macaca nemestrina* or *fascicularis* eyes were enucleated and hemisected to remove the anterior pole including the lens and vitreous humor. The retina, choroid and pigment epithelium were dissected as a unit from the sclera. Radial cuts were made to flatten the retina and it was fixed to a recording chamber with poly-L-

lysine, vitreal side up. The chamber was mounted in an upright microsope. The retina was superfused with oxygenated Ames medium and maintained at 36 °C. The pH of the Ames was adjusted to 7.4 at RT, while bubbling with 95% O2/5% CO2. Ames was supplemented with the pH buffer HEPES was adjusted to pH 7.4 under the same conditions. Pharmacological agents were added to the bath superfusion. All pharmacological agents were obtained from Sigma (St Louis, MO).

Electrical Recording

Glass microelectrodes (R = 250-500 MΩ) were filled with 2% Neurobiotin and 2% pyranine in 1M KCl. Retinas were stained with the vital dye acridine orange (several drops of 50 μM solution were added to the bath) and visualized with fluorescence episcopic illumination simultaneously with the microelectrode. Small bistratified ganglion cell bodies were targeted based upon size and shape of their somas located in the ganglion cell layer. Identity of recorded cells were confirmed after iontophoresis of pyranine allowed the examination of dendritic morphology in vitro. The electrode tip was positioned next to the soma and penetration was achieved using the amplifier's buzz feature. Intracellular voltage was amplified (Axoprobe 2B, Axon Instruments, Sunnyvale, CA) and digitized at 10 KHz. Data acquisition was controlled by custom software.

Visual Stimuli

Visual stimuli were generated by a digital light projector (DLP, VistaGRAPHX 2500, Christie Digital, Cypress, CA) controlled by custom software through a VSG3 stimulus generator (Cambridge Research Systems, England)(Packer et al., 2001). Stimuli

were focused through a 4x objective onto the retina. The retinal area covered by the stimulus was 2.96 X 2.22 mm. Chromatic stimuli were generated as previously described (Dacey et al., 2000b; Packer et al., 2001). In brief, the sum and mean intensities of the three DLP primaries were set to produce the same mean quantal catch in all three cone types of X photons/μm^2, holding mean cone adaptation levels constant. The intensity of each DLP primary was modulated above and below the mean contrast to produce modulation in either S cones or L and M cones. Multiple cycles of 2.03 Hz square wave modulated 2 mm diameter spots (for test responses) or drifting sinusoidal gratings (for receptive field measurements) were presented and averaged, and response amplitude was measured as the Fourier component of the voltage response at the stimulus frequency.

Gaussian Receptive Field Model

The responses of small bistratified cells to drifting gratings were fit with a linear Gaussian receptive field model as previously described (Enroth-Cugell et al., 1983; Dacey et al., 2000a; McMahon et al., 2004). Briefly, the receptive field center with a radial profile C(r) was described by the equation

$$C(r) = W_c \cdot \frac{1}{\pi} \cdot \left(\frac{1}{R_c}\right)^2 \cdot e^{(-r/R_c)^2},$$

where W_c is the gain of the center and R_c is the radius of the center (where sensitivity has fallen to 1/e of its peak). The amplitude of responses to stimulus modulation was computed as the two-dimensional integral of the product of the receptive field and stimulus profiles. Control responses to S and L+M gratings were fit with only a center, responses to L+M gratings in the presence of L-AP4 were fit with a center and a surround

S(r), with gain W_s and radius R_s. The overall amplitude and phase of the responses were computed by combining the center, and if appropriate, the surround responses with the equation

$$R = \left(A_c \cdot e^{(i\cdot\theta_c)}\right) + \left(A_s \cdot e^{(i\cdot\theta_s)}\right),$$

where A_c and A_s are the amplitudes of center and surround responses and θ_c and θ_s are the phases of their responses at the temporal frequency of the stimulus modulation. Initial fitting parameters were manually set and Numerical search (Grace, 1990) was used to minimize the mean square difference between the measured and predicted responses.

Results

Receptive Field

We first mapped the S ON and L+M OFF spatial receptive fields of small bistratified cells by measuring their spatial frequency response to drifting sinusoidal gratings that modulated either S cones, or L and M cones. In response to both S cone and L+M cone modulating gratings, small bistratified cell responses were low pass as a function of spatial frequency (Fig 22B, circles). This is in contrast to cells with center-surround receptive field structure, which exhibit band pass spatial frequency response profiles. The L+M responses fell off at lower spatial frequencies than the S responses. Both the S ON and L+M OFF spatial frequency responses were well fit with a Gaussian receptive field model (Fig 22B, lines). The Gaussian radius of the S ON receptive field was 116 ± 5 μm, and the radius of the L+M OFF receptive field was 157 ± 13 μm (Fig 22C), which was significantly larger than the S ON field ($p = 0.005$, $n=13$).

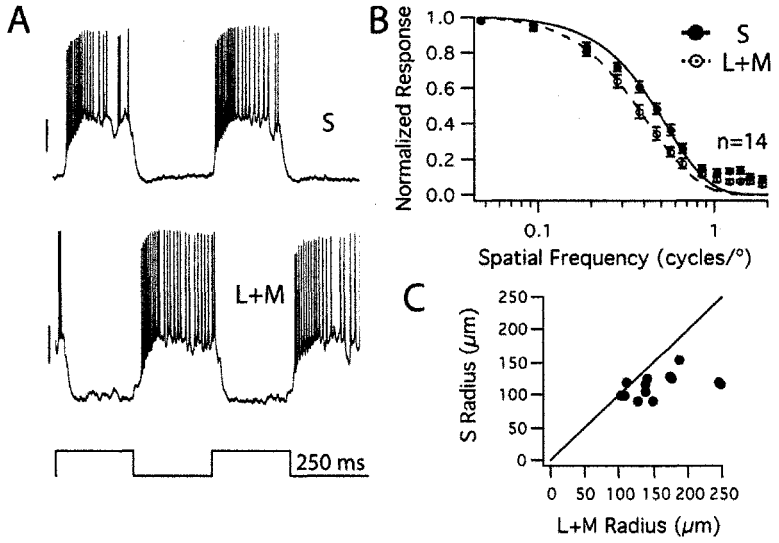

Figure 22: Small bistratified cell receptive field.
A: Responses to a 2000 μm spot of light flashed on and off at 250 ms intervals (stimulus trace below) that modulates S cones (above) or L and M cones (below). The cell responds at the onset of the S cone stimulus and the offset of the L+M cones stimulus. Scale bars = 10 mV. **B:** Response amplitude, measured as the Fourier component of the voltage response at the stimulus frequency, normalized to the maximum response, plotted as a function of spatial frequency of sinusoidal gratings drifting at 2 Hz that modulate S cones (filled circles) or L and M cones (open circles). Lines are Gaussian fits to S (solid) and L+M (dashed) data. N=13. The responses to L+M cone gratings falls off as lower spatial frequencies. **C:** Gaussian receptive field radius for the S response plotted against the Gaussian radius of the L+M response for 13 cells. Radii were predicted from the Gaussian fits in B. The L+M OFF receptive field radius was almost always larger the S ON radius.

L-AP4

To distinguish whether ON and OFF pathway inputs generate the S ON and L+M OFF responses, respectively, or if the LM-OFF responses are already present in the S ON input, we measured the responses to S cone and L+M cone modulating stimuli in the presence of the ON pathway blocker L-AP4. In the presence of 100 μM L-AP4, the S ON

Figure 23: L-AP4 abolishes the S ON and attenuates the L+M OFF light responses.
A: Responses of a small bistratified ganglion cell to a 2000 μm spot flashed on and off at 250 ms intervals that modulates S cones in the absence (above) and presence (below) of L-AP4. L-AP4 abolishes the S ON response. Scale bars = 10 mV.
B: Responses of a small bistratified ganglion cell to a 2000 μm spot flashed on and off at 250 ms intervals that modulates L and M cones in the absence (above) and presence (below) of L-AP4. L-AP4 attenuates the L+M OFF response. Scale bars = 10 mV.
C: Control response amplitude plotted against L-AP4 response amplitude for the S ON responses (above) and L+M OFF responses (below) for 9 cells. Amplitude was measured as the Fourier component of the voltage response at the stimulus frequency.
D: Normalized response amplitude plotted as a function of spatial frequency of sinusoidal gradings drifting at 2 Hz that modulate L and M cones in the absence (filled circles) and presence (open circles) of L-AP4. Lines are Gaussian fits to CTR (solid) and L-AP4 (dashed) data. N=4. In the presence of L-AP4 the spatial frequency response profile is bandpass, indicating center-surround receptive field profile.
E: Predicted L+M OFF center (empty) and L+M ON surround (filled) receptive field profile from fitting the spatial frequency responses from one cell with a difference of Gaussians receptive field model. Horizontal scale bar = 79 μm.

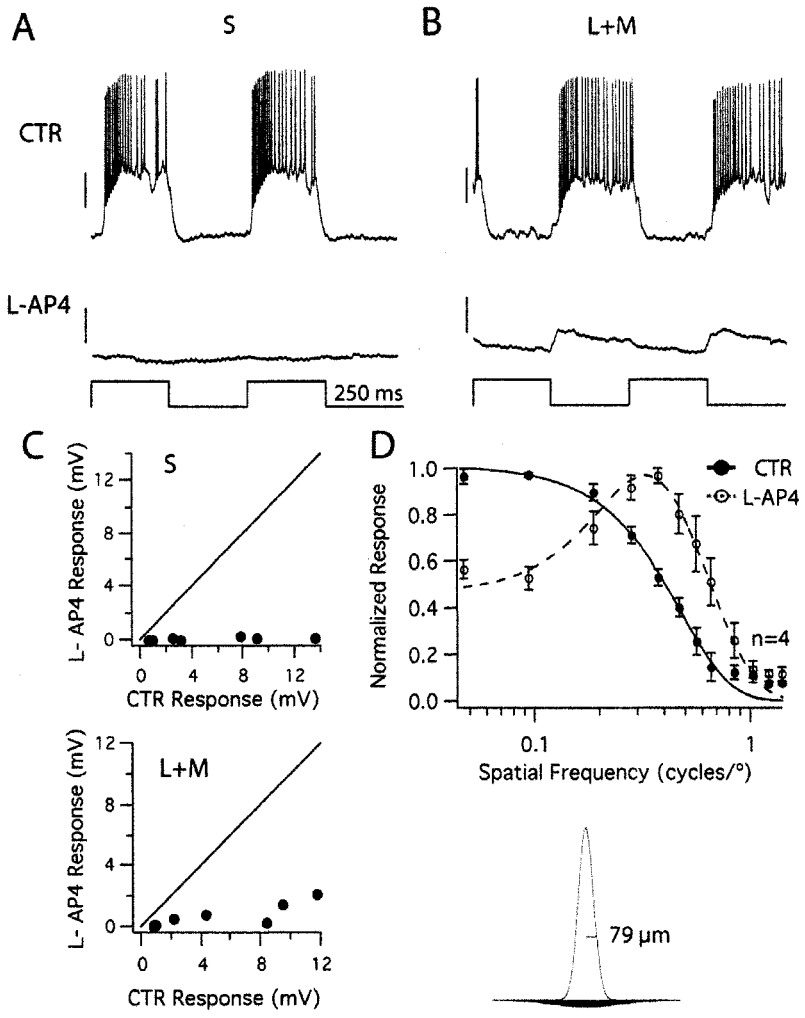
A
S
B
L+M
CTR
L-AP4
250 ms
C
S
L- AP4 Response (mV)
CTR Response (mV)
L+M
L- AP4 Response (mV)
CTR Response (mV)
D
CTR
L-AP4
n=4
Normalized Response
Spatial Frequency (cycles/°)
79 µm

responses, quantified as the amplitude of the Fourier component of the voltage response at the stimulus frequency, were completely abolished (Fig 23B, C) (L-AP4/CTR = 0.03 ± 0.01, n=9). The L+M OFF responses were significantly attenuated, though not completely abolished (Fig 23B, C) (L-AP4/CTR = 0.16 ± 0.02, n=9). These results are consistent with the ON pathway generating the S ON responses, but inconsistent with the OFF pathway generating the majority of the L+M OFF responses.

In the cases where the remaining L+M OFF response in the presence of L-AP4 was large enough, we mapped its spatial receptive field with L+M cone modulating drifting sinusoidal gratings. In contrast to the low pass spatial frequency profile in control (Fig 22B), in the presence of L-AP4 the spatial frequency profile was band pass, indicative of center-surround antagonism, and fell off at higher spatial frequencies, indicating a smaller receptive field center size (Fig 23D). The receptive field of the L+M OFF response in the presence of L-AP4 was well fit with a difference of Gaussians receptive field model with an L+M OFF center and L+M ON surround (Fig 23D, dashed line). The Gaussian radius of the center was 117 ± 18 μm, and the radius of the surround was 247 ± 39 μm (n=4). Thus, the L-AP4 resistant response to L+M stimuli likely represents the direct OFF bipolar cell input small bistratified cells receive.

Role of inhibitory inputs

To test what role inhibitory inputs play in the generation of the small bistratified light response, we measured the light responses in the presence of picrotoxin (PTX), which blocks GABA receptors, and strychnine (STR), which blocks glycine receptors. In

the presence of 100 μM PTX, the S ON and L+M OFF responses were both increased in amplitude, quantified as the amplitude Fourier component of the voltage response at the

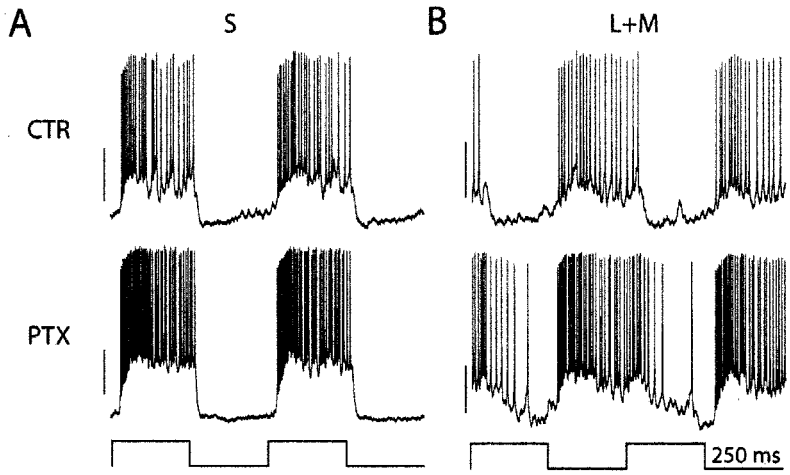

Figure 24: Picrotoxin increases response amplitude.
A: Responses of a small bistratified ganglion cell to a 2000 μm spot flashed on and off at 250 ms intervals that modulates S cones in the absence (above) and presence (below) of PTX. PTX increases the amplitude of the S ON response. Scale bars = 10 mV.
B: Responses of a small bistratified ganglion cell to a 2000 μm spot flashed on and off at 250 ms intervals that modulates L and M cones in the absence (above) and presence Scale bars = 10 mV. (below) of PTX. PTX increases the amplitude and broadens the L+M OFF response.

stimulus frequency (Fig 24A, B)(PTX/CTR S = 1.63 ± 0.14, L+M = 1.44 ± 0.22, n=3). The L+M OFF responses also hyperpolarized more slowly at the onset of the light stimulus (Fig 24B). The width of the L+M response, measured at 1/3 the maximum response amplitude, increased from 264 ± 10 ms to 316 ± 13 ms (n=3). The width of the S response was unchanged, from 246 ± 4 ms to 245 ± 8 ms (n=3). In the presence of 2 μM STR, the light responses were not significantly changed in amplitude (Fig 25A, B) (STR/CTR S = 0.92 ± 0.12, L+M = 1.04 ± 0.07, n=3) or width (S CTR = 241 ± 6 ms, S STR = 243 ± 8 ms; L+M CTR = 257 ± 14 ms, L+M STR = 252 ± 19 ms, n=3).

GABAergic inhibition thus appears to modulate the response, and glycinergic inhibition does not have a significant role in generating the basic light response of small bistratified cells.

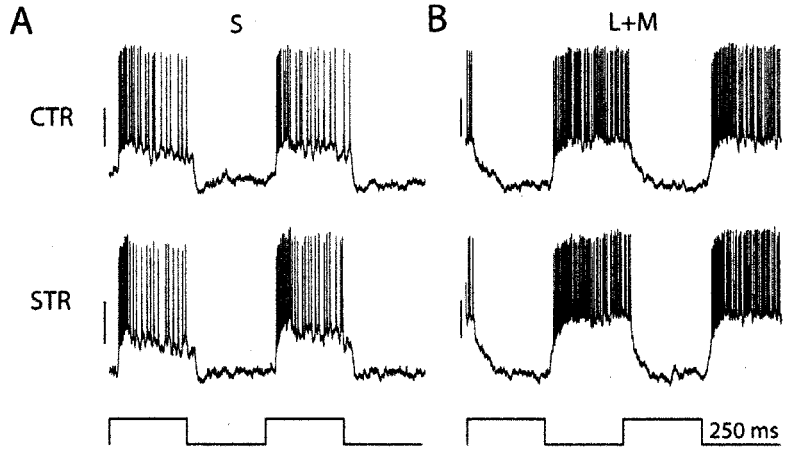

Figure 25: Strychnine does not affect the light response.
A: Responses of a small bistratified ganglion cell to a 2000 μm spot flashed on and off at 250 ms intervals that modulates S cones in the absence (above) and presence (below) of STR. STR does not affect the S ON response. Scale bars = 10 mV. **B:** Responses of a small bistratified ganglion cell to a 2000 μm spot flashed on and off at 250 ms intervals that modulates L and M cones in the absence (above) and presence (below) of STR. STR does not affect the L+M OFF response. Scale bars = 10 mV.

Role of outer retinal feedback

To test what role outer retinal feedback mediated by horizontal cells has in generating the light response of small bistratified cells we measured the responses in the presence of the pH buffer HEPES, which has been shown to attenuate horizontal cell feedback to cones and primate parasol ganglion cell surrounds. In the presence of 20 mM HEPES, S ON responses were increased in amplitude (Fig 26A, C) (HEPES/CTR = 1.68 ± 0.39, n=7). In 5/7 cells, the L+M OFF responses were significantly attenuated (Fig 26C, closed circles) (HEPES/CTR = 0.38 ± 0.08) and a transient L+M ON component was apparent (Fig 26B). In 2/7 cells the responses were completely inverted to a pure

L+M ON responses (Fig 26C, open circles). These results suggest that outer retinal feedback serves a critical role in generating the L+M OFF responses of small bistratified cells.

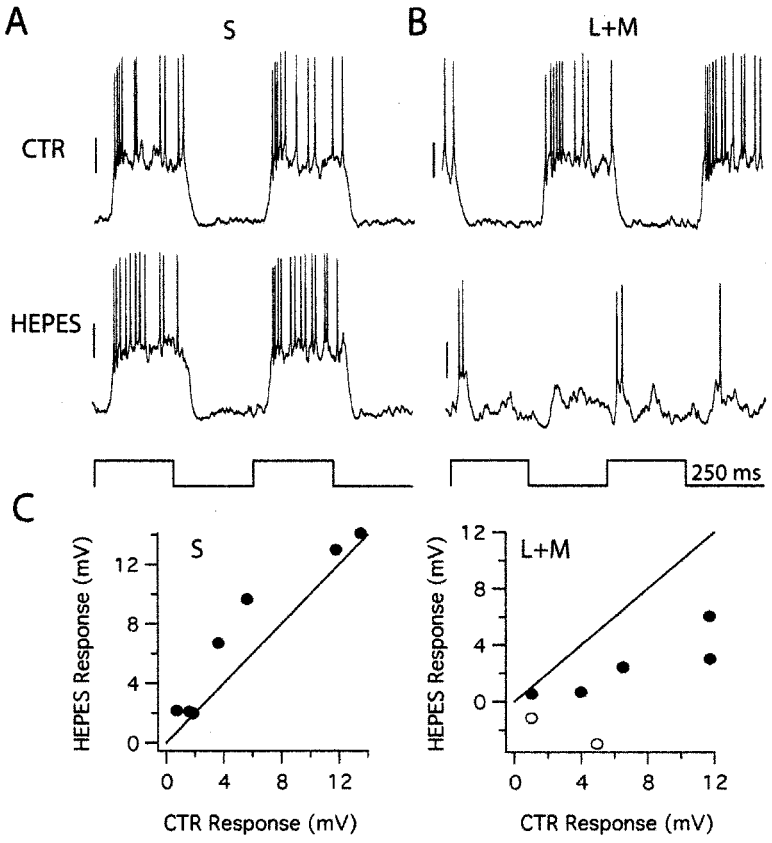

Figure 26: HEPES selectively attenuates the L+M OFF response.
A: Responses of a small bistratified ganglion cell to a 2000 μm spot flashed on and off at 250 ms intervals that modulates S cones in the absence (above) and presence (below) of HEPES. HEPES slightly increases S ON response. Scale bars = 10 mV. **B:** Responses of a small bistratified ganglion cell to a 2000 μm spot flashed on and off at 250 ms intervals that modulates L and M cones in the absence (above) and presence (below) of HEPES. HEPES attenuates the L+M OFF response. Scale bars = 10 mV. **C:** Control response amplitude plotted against HEPES response amplitude for the S ON responses (left) and L+M OFF responses (right) for 7 cells. In two of the cells the L+M OFF responses were inverted to L+M ON responses, represented as negative values (open circles).

Discussion

We have shown that the basic L+M OFF light response in the primate small bistratified ganglion cell is sensitive to L-AP4 and HEPES, and not sensitive to PTX or STR. This supports a new picture of small bistratified cell circuitry in which the yellow OFF response is generated predominantly by the ON pathway in the outer retina as a conventional surround of S cones. A small amount of the L+M OFF response is L-AP4 resistant, and has its own L+M OFF center and L+M ON surround. We propose that this input modulates the S ON center- L+M OFF surround type I receptive field present in S

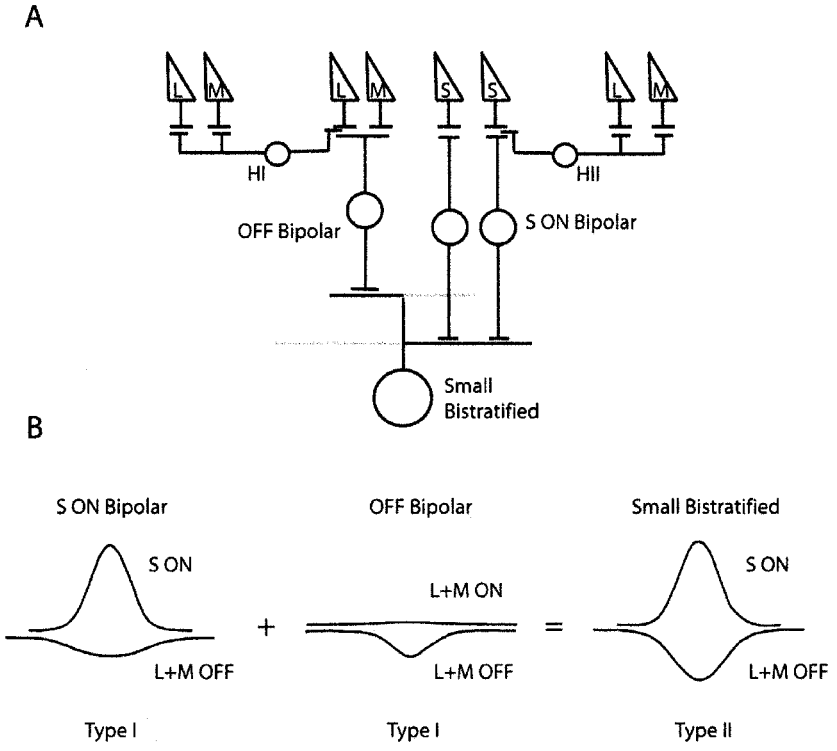

Figure 27: Proposed small bistratified cell circuitry.
A: Small bistratified ganglion cells receive input from S ON bipolar cells, with type I S ON center/L+M OFF surround receptive field and diffuse OFF bipolar cells with type I L+M OFF center/L+M ON surround receptive field. **B:** These receptive fields combine to produce the type II S ON/L+M OFF receptive field.

cones and S ON bipolar cells, creating a type II receptive field in the small bistratified cell (Fig 27).

The hypothesis that the small bistratified cell generated its blue-yellow opponent physiology using S ON pathway input and L+M OFF pathway input to its inner and outer dendritic trees, respectively, was logical and was attractive in its simplicity. However, morphological analysis of the inner and outer dendritic trees and the number of bipolar cell inputs to each was not completely consistent with this hypothesis. The primate small bistratified cell inner dendritic tree is larger and more highly branched than the outer dendritic tree (Dacey, 1993; Dacey and Lee, 1994; Silveira et al., 1999). Electron microscopy studies in the primate retina have shown that the outer tree receives significantly less bipolar cell input than the inner tree. In the macaque fovea, the outer tree receives about half as many bipolar cell inputs as the inner tree (Calkins et al., 1998). In the peripheral marmoset retina, the outer tree received less than one tenth the number of bipolar cell inputs, and the bipolar cell input to the outer tree represents only ~ 1 % of the total synaptic input (Ghosh and Grunert, 1999). The differences between these studies is likely due to the different eccentricities of the cells examined, but both show that there is a smaller number of bipolar cell inputs to the outer tree, which is inconsistent with the equal size of the S ON and L+M OFF responses. Our finding that the L+M OFF response that is resistant to L-AP4 is ~ 15 % of the control response amplitude is consistent with the small bistratified cell morphology and is consistent with the hypothesis that the yellow OFF response is not generated predominantly by OFF pathway input.

Our new model of small bistratified circuitry rests strongly on the affect of L-AP4 on the L+M OFF response. The interpretation that the majority of the L+M OFF response

is generated by the ON pathway is dependent on the assumption that L-AP4 is a selective ON pathway blocker (Slaughter and Miller, 1981). L-AP4 is a group III metabotropic glutamate receptor (mGluR) agonist (Conn and Pin, 1997). mGluR6 is the L-AP4 target at the photoreceptor-ON bipolar cell synapse, and this is the only location of mGluR6 in the primate retina (Vardi et al., 2000). However, other group III mGluRs are present in vertebrate retina, (Brandstatter, 2002; Gerber, 2003) and mGluR4a and mGluR8 have similar sensitivity to L-AP4 (Conn and Pin, 1997). In rat and mouse these receptors are expressed predominantly in the inner plexiform layer (Koulen et al., 1996; Quraishi et al., 2007), and are thought to serve a modulatory role. There is evidence for L-AP4 inhibition of OFF pathway responses in the salamander retina (Awatramani and Slaughter, 2001; Higgs et al., 2002). However, these affects were strongest at low light levels in dark-adapted retina, and at higher light levels L-AP4 increased OFF responses. Many studies in multiple species have shown that L-AP4 does not change or increases response amplitude of OFF ganglion cells and the OFF component of ON-OFF ganglion cells and ON-OFF amacrine cells (Horton and Sherk, 1984; Cohen, 1998; Popova et al., 2003). In addition there is evidence that OFF pathway cells are inhibited by the ON pathway (Roska and Werblin, 2001) and relief of this inhibition caused by blocking the ON pathway would strengthen OFF pathway responses. We can't exclude the possibility that L-AP4 acts directly on OFF pathway cells, but in our primate retina preparation we have never seen a strong effect of L-AP4 on OFF pathway responses. In the ON-OFF A1 amacrine cell, L-AP4 selectively blocks ON center responses, with no effect on OFF center responses (Davenport et al., 2007). The drastic change in the spatial receptive field in the presence of L-AP4 is also inconsistent with a general block of the OFF pathway. If

L-AP4 decreased the gain of the OFF pathway, the responses should be decreased in size, but the receptive field should properties should remain the same. In addition, both the smaller outer dendritic tree of small bistratified cells, and the effect of HEPES (see below) are consistent with the effect of L-AP4 in suggesting that small bistratified cells receive a relatively small amount of direct OFF pathway input.

HEPES attenuates horizontal cell feedback to cones in goldfish retina (Hirasawa and Kaneko, 2003; Vessey et al., 2005a; Cadetti and Thoreson, 2006). In primate retina, HEPES attenuates the surrounds of parasol ganglion cells, and the slow depolarization of the horizontal cell light response, both of which are thought to be generated by horizontal cell feedback (Davenport et al, 2007). Other pH buffers also attenuate the slow depolarization of the horizontal cell light response. These experiments are consistent with HEPES acting to block horizontal cell feedback to cones via its pH buffering properties, and support our interpretation that HEPES is interfering with HII horizontal cell feedback to S cones in the present study.

The HII horizontal cell is the only horizontal cell type in the primate retina that selectively and densely contacts S cones. It also contacts L and M cones, though sparsely. It was initially rejected as a candidate for mediating blue-yellow opponency because it hyperpolarizes in response to stimulation of all three cone types, and does not itself exhibit an opponent physiology (Dacey et al., 1996). Our finding that HEPES attenuates only the L+M OFF response of small bistratified cells suggests that the HII horizontal cell does in fact mediate opponency.

Because no S cone signal is observable in non-chromatic ganglion cells, such as parasol cells (Sun et al., 2006), that receive input from both L and M cones, this suggests

that while the HII receives input form all three cone types, it must only be capable of providing output to S cones. In fact, the dendritic terminals of HII cells are smaller and thinner than HI horizontal cells, and they make many more contacts with S cones that L and M cones (Ahnelt and Kolb, 1994b, 1994a). This morphological disparity could form the basis for unidirectional feedback. The synaptic mechanism of feedback is not clear, and could rely on dense horizontal cell innervation. There could also only be feedback machinery present at dendritic terminals that contact S cones.

Electron microscopy of small bistratified cells in the peripheral marmoset retina suggest that they receive a large amount of input, presumably inhibitory, from amacrine cells (Ghosh and Grunert, 1999). Our results with picrotoxin and strychnine suggest that while inhibitory inputs do not have a central role in generating the basic light response of small bistratified cells, they do serve a modulatory role. GABAergic inputs appear to control the gain of both the S ON and L+M OFF light responses, and the kinetics of some parts of the light response. It is also likely that the effect of amacrine cell input is not fully appreciated based on the simple stimuli used in this study.

We propose that HII horizontal cells in the outer retina feedback from L and M cones to S cones creating an L+M surround in S cones that is transferred to ON S cone bipolar cells which represent the majority of bipolar cell input to small bistratified cells. Alone, this input would produce a type I receptive field in small bistratified cells with a narrow blue ON center and a broad yellow OFF surround. By adding a small amount of OFF bipolar cell input with a narrow L+M OFF center and broad L+M ON surround, the combined L+M OFF center of the OFF bipolar cell input and L+M OFF surround of the ON bipolar cell input create a region of increased gain at the center of the receptive field,

and the broad L+M OFF surround decreases the gain in the periphery of the receptive field, yielding a more type-II like yellow OFF receptive field in the small bistratified cell (Fig 27).

Chapter 4: Future Experiments

A1 Amacrine cells

The most important piece of information that needs to be established is what the postsynaptic target(s) of the A1 amacrine cell axons are. Placing the A1 cell within the context of a complete retinal circuit will provide a clearer picture of its functional role and will better direct future experiments to understand its role in visual processing. The starburst amacrine cell, for example, has generated sustained interest and study because it is known to be associated with the direction selective ganglion cell and its involvement in direction selectivity (reviewed in Vaney and Taylor, 2002).

The axons of the A1 amacrine cell stratify in the center of the IPL, and it has been shown that a subset of ganglion cells in rabbit retina whose dendrites also stratify in the center of the IPL receive inhibitory input during global image motion, but those whose dendrites stratify more distally or proximally in the IPL do not (Roska and Werblin, 2003). The broad thorny cell mentioned in chapter 1 is one possible target in the primate retina. Another possibility is an alpha-like ganglion cell in the primate retina recently identified from retrograde tracing from the LGN (unpublished data, DM Dacey). Both of these cells have dendrites that stratify in the center of the IPL and display transient light responses that would be appropriately inhibited by the transient A1 amacrine output. Both also would be logical targets for saccadic suppression, as they would be expected to respond strongly to quickly moving stimuli. A first step in testing if they are, in fact, A1 axon targets would be to probe them both within and outside of their classical receptive fields with stimuli that strongly excite A1 amacrine cells and examine whether they

receive inhibition that is consistent with the A1 amacrine cell. The effect of agents that would be expected to block A1 amacrine cell axonal output on the light responses of these cells could be examined as well. TTX, for example, should block A1 axonal action potentials and PTX should block GABAergic output of A1 cells. Though technically challenging, A1 cells and nearby ganglion cells could be filled with dye and the colocalization of A1 axons and ganglion cell dendrites could be examined. It would be expected that the bouton-like swellings of the A1axons would be colocalized with appropriate ganglion cell dendrites.

Horizontal cell feedback

The results described in chapter 2 are consistent with horizontal cell feedback to cones requiring local pH changes in the outer retina. pH sensitive electrodes have been used in the retina to measure local pH (Borgula et al., 1989; Oakley and Wen, 1989; Yamamoto et al., 1992) but the restricted nature of the cone pedicle makes it unlikely that they could be used to detect the spatially localized pH changes predicted by the pH model of horizontal cell feedback. To overcome this limitation, two-photon imaging of florescent dyes that are sensitive to pH could be performed (Bevensee and Boron, 1998a). Dyes could be applied extracellularly and labeling of horizontal cell dendrites and/or cone axon terminals could be used to localize the cone synaptic cleft in the OPL. It should then be possible to detect changes in the synaptic cleft in response to light and in response to modulation of horizontal cell membrane voltage.

The mechanism linking horizontal cell voltage to pH changes in the cone pedicle has not been identified. The pH hypothesis maintains that the synaptic cleft is acidic in

darkness, and basic in light. In darkness, constant exocytosis of acidic synaptic vesicles from cone axon terminals contributes to lowering the pH of the cleft (DeVries, 2001), and the decrease of vesicular release caused by light will contribute to increasing the cleft pH. Horizontal cells are depolarized in darkness and hyperpolarized in light. They could create the appropriate pH changes in the synaptic cleft either by an extrusion of protons that is caused by depolarization or an influx of protons caused by hyperpolarization. Glutamate-dependent proton fluxes have been measured outside isolated horizontal cells using proton-sensitive electrodes, but glutamate decreases the extracellular concentration of protons, which is not consistent with the pH model of feedback (Molina et al., 2000; Molina et al., 2004). Proton channels (Decoursey, 2003) as well as a number of proton and bicarbonate pumps and exchangers (Bevensee and Boron, 1998b) are known to exist that could contribute to appropriate voltage dependent proton fluxes in the cone synaptic cleft. There are pharmacological agents that target many of these mechanisms (Bevensee and Boron, 1998b), and their effect on horizontal cell feedback could be determined.

Opponency in small bistratified cells

The experiments described in chapter 3 sugested that blue-yellow opponency in primeate small bistratified ganglion cells is generated predominantly in the outer retina by HII horizontal cell feedback from L and M cones to S cones. This predicts that both S cones and S cone bipolar cells will exhibit L+M OFF surrounds. S cones are accessible in the primate retina and the chromatic properties of their receptive fields can be tested. S cone bipolar cells are not easily identifiable for targeted recording in the primate retina. We also predict that the small amount of L+M OFF bipolar cell input serves to modulate

the spatial properties of the S ON input to create a type II receptive field in small bistratified cells. This suggests that the L+M OFF surround of both cones and bipolar cells will be a type I conventional surround.

Whole cell voltage clamp of small bistratified cells should also be informative. Our results suggest that the excitatory inputs at the onset of a blue light stimulus will exhibit opponency, and that the excitatory inputs at the offset of a yellow light will be smaller and will exhibit center-surround receptive field organization. Inhibitory inputs could also be isolated and studied to verify that they do not carry an opponent signal, as predicted by our data. Their magnitude and temporal properties could also clarify their role in the small bistratified cell circuit.

Horizontal cell feedback from L and M cones to S cones must be unidirectional, despite the fact that HII horizontal cells hyperpolarize in response to modulation of all three cone types. Blocking feedback with HEPES could have differential effects on the responses of HII horizontal cells to S and L+M stimuli that could indicate unidirectional feedback. The HII-S cone contacts are denser and more elaborated than the HII-L/M cone contacts and this difference is recognizable with practice. Labeling of HII horizontal cells could be used in combination with extracellular pH imaging to determine if modulation of HII horizontal cell membrane potential causes an associated pH change in the pedicle of only S cones and not L and M cones.

References

Ahnelt P, Kolb H (1994a) Horizontal cells and cone photoreceptors in primate retina: a Golgi-light microscopic study of spectral connectivity. J Comp Neurol 343:387-405.

Ahnelt P, Kolb H (1994b) Horizontal cells and cone photoreceptors in human retina: a Golgi-electron microscopic study of spectral connectivity. J Comp Neurol 343:406-427.

Ambrose JM, Hayhoe MM (1980) Surround configuration and cone dark adaptation. Vision Research 20:883.

Awatramani GB, Slaughter MM (2001) Intensity-dependent, rapid activation of presynaptic metabotropic glutamate receptors at a central synapse. J Neurosci 21:741-749.

Ayoub GS, Lam DM (1984) The release of gamma-aminobutyric acid from horizontal cells of the goldfish (Carassius auratus) retina. J Physiol 355:191-214.

Barnes S (2003) Center-surround Antagonism Mediated by Proton Signaling at the Cone Photoreceptor Synapse. J Gen Physiol 122:653-656.

Barnes S, Bui Q (1991) Modulation of calcium-activated chloride current via pH-induced changes of calcium channel properties in cone photoreceptors. J Neurosci 11:4015-4023.

Baylor DA, Fuortes MG, O'Bryan PM (1971) Receptive fields of cones in the retina of the turtle. J Physiol 214:265-294.

Bevans CG, Harris AL (1999) Regulation of Connexin Channels by pH. Direct action of the protonated form of taurine and other aminosulfonates. J Biol Chem 274:3711-3719.

Bevensee M, Boron W (1998a) Fluorescence indicators. In: pH and brain function. (Kaila K, Ranson BR, eds), pp 129-151. New York: John Wiley & Sons.

Bevensee M, Boron W (1998b) pH regulation in mammalian neurons. In: pH and brain function. (Kaila K, Ranson BR, eds), pp 211-231. New York: John Wiley & Sons.

Bloomfield SA (1996) Effect of spike blockade on the receptive-field size of amacrine and ganglion cells in the rabbit retina. J Neurophysiol 75:1878-1893.

Bolz J, Frumkes T, Voigt T, Wassle H (1985) Action and localization of gamma-aminobutyric acid in the cat retina. J Physiol 362:369-393.

Borgula GA, Karwoski CJ, Steinberg RH (1989) Light-evoked changes in extracellular pH in frog retina. Vision Res 29:1069-1077.

Brandstatter JH (2002) Glutamate receptors in the retina: the molecular substrate for visual signal processing. Curr Eye Res 25:327-331.

Burns ME, Arshavsky VY (2005) Beyond Counting Photons: Trials and Trends in Vertebrate Visual Transduction. Neuron 48:387.

Burr D (2004) Eye movements: keeping vision stable. Curr Biol 14:R195-197.

Byzov AL, Shura-Bura TM (1986) Electrical feedback mechanism in the processing of signals in the outer plexiform layer of the retina. Vision Res 26:33-44.

Cadetti L, Thoreson WB (2006) Feedback Effects of Horizontal Cell Membrane Potential on Cone Calcium Currents Studied With Simultaneous Recordings. J Neurophysiol 95:1992-1995.

Calkins DJ (2005) Localization of ionotropic glutamate receptors to invaginating dendrites at the cone synapse in primate retina. Vis Neurosci 22:469-477.

Calkins DJ, Tsukamoto Y, Sterling P (1998) Microcircuitry and mosaic of a blue-yellow ganglion cell in the primate retina. J Neurosci 18:3373-3385.

Callaway EM (2005) Structure and function of parallel pathways in the primate early visual system. J Physiol (Lond) 566:13-19.

Chesler M (1998) Principles and practical aspects of pH buffering. In: pH and brain function. (Kaila K, Ranson BR, eds), pp 11-20. New York: John Wiley & Sons.

Cohen ED (1998) Interactions of inhibition and excitation in the light-evoked currents of X type retinal ganglion cells. J Neurophysiol 80:2975-2990.

Conn PJ, Pin JP (1997) Pharmacology and functions of metabotropic glutamate receptors. Annu Rev Pharmacol Toxicol 37:205-237.

Dacey D, Packer OS, Diller L, Brainard D, Peterson B, Lee B (2000a) Center surround receptive field structure of cone bipolar cells in primate retina. Vision Res 40:1801-1811.

Dacey DM (1988) Dopamine-accumulating retinal neurons revealed by in vitro fluorescence display a unique morphology. Science 240:1196-1198.

Dacey DM (1989) Axon-bearing amacrine cells of the macaque monkey retina. J Comp Neurol 284:275-293.

Dacey DM (1990) The dopaminergic amacrine cell. J Comp Neurol 301:461-489.

Dacey DM (1993) Morphology of a small-field bistratified ganglion cell type in the macaque and human retina. Vis Neurosci 10:1081-1098.

Dacey DM (1994) Physiology, morphology and spatial densities of identified ganglion cell types in primate retina. Ciba Found Symp 184:12-28; discussion 28-34, 63-70.

Dacey DM (1996) Circuitry for color coding in the primate retina. Proc Natl Acad Sci U S A 93:582-588.

Dacey DM, Lee BB (1994) The 'blue-on' opponent pathway in primate retina originates from a distinct bistratified ganglion cell type. Nature 367:731.

Dacey DM, Diller LC, Verweij J, Williams DR (2000b) Physiology of L- and M-cone inputs to H1 horizontal cells in the primate retina. J Opt Soc Am A Opt Image Sci Vis 17:589-596.

Dacey DM, Peterson BB, Robinson FR, Gamlin PD (2003) Fireworks in the Primate Retina: In Vitro Photodynamics Reveals Diverse LGN-Projecting Ganglion Cell Types. Neuron 37:15.

Dacey DM, Lee BB, Stafford DK, Pokorny J, Smith VC (1996) Horizontal Cells of the Primate Retina: Cone Specificity Without Spectral Opponency. Science 271:656-659.

Daw NW, Ariel M (1981) Effect of synaptic transmitter drugs on receptive fields of rabbit retinal ganglion cells. Vision Res 21:1643-1647.

De Valois RL, Smith CJ, Kitai ST, Karoly AJ (1958) Response of single cells in monkey lateral geniculate nucleus to monochromatic light. Science 127:238-239.

Decoursey TE (2003) Voltage-gated proton channels and other proton transfer pathways. Physiol Rev 83:475-579.

Denk W, Detwiler PB (1999) Optical recording of light-evoked calcium signals in the functionally intact retina. PNAS %R 101073/pnas96127035 96:7035-7040.

Denk W, Strickler JH, Webb WW (1990) Two-Photon Laser Scanning Fluorescence Microscopy. Science 248:73.

DeVries SH (2001) Exocytosed protons feedback to suppress the Ca2+ current in mammalian cone photoreceptors. Neuron 32:1107-1117.

Dowling JE (1970) Organization of vertebrate retinas. Invest Ophthalmol 9:655-680.

Enroth-Cugell C, Robson JG, Schweitzer-Tong DE, Watson AB (1983) Spatio-temporal interactions in cat retinal ganglion cells showing linear spatial summation. J Physiol 341:279-307.

Euler T, Detwiler PB, Denk W (2002) Directionally selective calcium signals in dendrites of starburst amacrine cells. Nature 418:845-852.

Famiglietti EV (1992a) Polyaxonal amacrine cells of rabbit retina: morphology and stratification of PA1 cells. J Comp Neurol 316:391-405.

Famiglietti EV (1992b) Polyaxonal amacrine cells of rabbit retina: size and distribution of PA1 cells. J Comp Neurol 316:406-421.

Famiglietti EV (1992c) Polyaxonal amacrine cells of rabbit retina: PA2, PA3, and PA4 cells. Light and electron microscopic studies with a functional interpretation. J Comp Neurol 316:422-446.

Flores-Herr N, Protti DA, Wassle H (2001) Synaptic currents generating the inhibitory surround of ganglion cells in the mammalian retina. J Neurosci 21:4852-4863.

Freed MA, Pflug R, Kolb H, Nelson R (1996) ON-OFF amacrine cells in cat retina. J Comp Neurol 364:556-566.

Frishman LJ, Linsenmeier RA (1982) Effects of picrotoxin and strychnine on non-linear responses of Y-type cat retinal ganglion cells. J Physiol 324:347-363.

Geffen MN, de Vries SEJ, Meister M (2007) Retinal Ganglion Cells Can Rapidly Change Polarity from Off to On. PLoS Biology 5:e65.

Gerber U (2003) Metabotropic glutamate receptors in vertebrate retina. Doc Ophthalmol 106:83-87.

Ghosh KK, Grunert U (1999) Synaptic input to small bistratified (blue-ON) ganglion cells in the retina of a new world monkey, the marmoset Callithrix jacchus. J Comp Neurol 413:417-428.

Goldberg JH, Tamas G, Yuste R (2003) Ca2+ imaging of mouse neocortical interneurone dendrites: Ia-type K+ channels control action potential backpropagation. J Physiol 551:49-65.

Good NE, Winget GD, Winter W, Connolly TN, Izawa S, Singh RM (1966) Hydrogen ion buffers for biological research. Biochemistry 5:467-477.

Grace A (1990) Optimization toolbox for use with Matlab: User's Guide. Natlick, MA: The Mathworks, Inc.

Hare WA, Owen WG (1998) Effects of bicarbonate versus HEPES buffering on measured properties of neurons in the salamander retina. Vis Neurosci 15:263-271.

Higgs MH, Romano C, Lukasiewicz PD (2002) Presynaptic effects of group III metabotropic glutamate receptors on excitatory synaptic transmission in the retina. Neuroscience 115:163-172.

Hirasawa H, Kaneko A (2003) pH Changes in the Invaginating Synaptic Cleft Mediate Feedback from Horizontal Cells to Cone Photoreceptors by Modulating Ca2+ Channels. J Gen Physiol 122:657-671.

Horton JC, Sherk H (1984) Receptive field properties in the cat's lateral geniculate nucleus in the absence of on-center retinal input. J Neurosci 4:374-380.

Hosoya T, Baccus SA, Meister M (2005) Dynamic predictive coding by the retina. Nature 436:71.

Janssen-Bienhold U, Schultz K, Gellhaus A, Schmidt P, Ammermuller J, Weiler R (2001) Identification and localization of connexin26 within the photoreceptor-horizontal cell synaptic complex. Vis Neurosci 18:169-178.

Kamermans M, Spekreijse H (1999) The feedback pathway from horizontal cells to cones: A mini review with a look ahead. Vision Research 39:2449.

Kamermans M, Fahrenfort I (2004) Ephaptic interactions within a chemical synapse: hemichannel-mediated ephaptic inhibition in the retina. Curr Opin Neurobiol 14:531-541.

Kamermans M, Fahrenfort I, Schultz K, Janssen-Bienhold U, Sjoerdsma T, Weiler R (2001) Hemichannel-Mediated Inhibition in the Outer Retina. Science 292:1178-1180.

Kaneko A (1971) Electrical connexions between horizontal cells in the dogfish retina. J Physiol 213:95-105.

Kaneko A, Stuart AE (1984) Coupling between horizontal cells in the carp retina revealed by diffusion of Lucifer yellow. Neurosci Lett 47:1-7.

Kaneko A, Tachibana M (1986) Effects of gamma-aminobutyric acid on isolated cone photoreceptors of the turtle retina. J Physiol 373:443-461.

Kolb H, Fernandez E, Schouten J, Ahnelt P, Lindberg KA, Fisher SK (1994) Are there three types of horizontal cell in the human retina? The Journal of Comparative Neurology 343:370-386.

Koulen P, Malitschek B, Kuhn R, Wassle H, Brandstatter JH (1996) Group II and group III metabotropic glutamate receptors in the rat retina: distributions and developmental expression patterns. Eur J Neurosci 8:2177-2187.

Kruger J, Fischer B, Barth R (1975) The shift-effect in retinal ganglion cells of the rhesus monkey. Exp Brain Res 23:443-446.

Kuffler SW (1953) Discharge patterns and functional organization of mammalian retina. J Neurophysiol 16:37-68.

Lev-Ram V, Grinvald A (1987) Activity-dependent calcium transients in central nervous system myelinated axons revealed by the calcium indicator Fura-2. Biophys J 52:571-576.

Marc RE, Stell WK, Bok D, Lam DM (1978) GABA-ergic pathways in the goldfish retina. J Comp Neurol 182:221-244.

Mariani AP (1989) Synaptic organization of classical neurotransmitter phenotypes in the primate retina. Neurosci Res Suppl 10:S101-116.

Mariani AP (1990) Amacrine cells of the rhesus monkey retina. J Comp Neurol 301:382-400.

Mariani AP, Cosenza-Murphy D, Barker JL (1987) GABAergic synapses and benzodiazepine receptors are not identically distributed in the primate retina. Brain Res 415:153-157.

Masland RH (2001) The fundamental plan of the retina. Nat Neurosci 4:877-886.

Massey SC, O'Brien JJ, Trexler EB, Li W, Keung JW, Mills SL, O'Brien J (2003) Multiple neuronal connexins in the mammalian retina. Cell Commun Adhes 10:425-430.

McMahon MJ, Packer OS, Dacey DM (2004) The classical receptive field surround of primate parasol ganglion cells is mediated primarily by a non-GABAergic pathway. J Neurosci 24:3736-3745.

Molina AJ, Smith PJ, Malchow RP (2000) Hydrogen ion fluxes from isolated retinal horizontal cells: modulation by glutamate. Biol Bull 199:168-170.

Molina AJ, Verzi MP, Birnbaum AD, Yamoah EN, Hammar K, Smith PJ, Malchow RP (2004) Neurotransmitter modulation of extracellular H+ fluxes from isolated retinal horizontal cells of the skate. J Physiol 560:639-657.

Nagelhus EA, Mathiisen TM, Bateman AC, Haug FM, Ottersen OP, Grubb JH, Waheed A, Sly WS (2005) Carbonic anhydrase XIV is enriched in specific membrane domains of retinal pigment epithelium, Muller cells, and astrocytes. Proc Natl Acad Sci U S A 102:8030-8035.

Naka KI, Rushton WA (1967) The generation and spread of S-potentials in fish (Cyprinidae). J Physiol 192:437-461.

Norton AL, Spekreijse H, Wolbarsht ML, Wagner HG (1968) Receptive field organization of the S-potential. Science 160:1021-1022.

O'Brien JJ, Li W, Pan F, Keung J, O'Brien J, Massey SC (2006) Coupling between A-Type Horizontal Cells Is Mediated by Connexin 50 Gap Junctions in the Rabbit Retina. J Neurosci %R 101523/JNEUROSCI2296-062006 26:11624-11636.

Oakley B, 2nd, Wen R (1989) Extracellular pH in the isolated retina of the toad in darkness and during illumination. J Physiol 419:353-378.

Ochrietor JD, Clamp MF, Moroz TP, Grubb JH, Shah GN, Waheed A, Sly WS, Linser PJ (2005) Carbonic anhydrase XIV identified as the membrane CA in mouse retina: strong expression in Muller cells and the RPE. Experimental Eye Research 81:492.

Oesch N, Euler T, Taylor WR (2005) Direction-Selective Dendritic Action Potentials in Rabbit Retina. Neuron 47:739.

Olveczky BP, Baccus SA, Meister M (2003) Segregation of object and background motion in the retina. Nature 423:401-408.

Packer O, Diller LC, Verweij J, Lee BB, Pokorny J, Williams DR, Dacey DM, Brainard DH (2001) Characterization and use of a digital light projector for vision research. Vision Research 41:427.

Packer OS, Dacey DM (2002) Receptive field structure of H1 horizontal cells in macaque monkey retina. Journal of Vision 2:272-292.

Packer OS, Dacey DM (2005) Synergistic center-surround receptive field model of monkey H1 horizontal cells. Journal of Vision 5:1038-1054.

Perlman I, Normann RA (1990) The effects of GABA and related drugs on horizontal cells in the isolated turtle retina. Vis Neurosci 5:469-477.

Polyak S (1941) The Retina. Chicaco, Il: University of Chicago Press.

Popova E, Mitova L, Vitanova L, Kupenova P (2003) Participation of the GABAergic system in the action of 2-amino-4-phosphonobutyrate on the OFF responses of frog retinal ganglion cells. Vision Res 43:607-616.

Quraishi S, Gayet J, Morgans CW, Duvoisin RM (2007) Distribution of group-III metabotropic glutamate receptors in the retina. J Comp Neurol 501:931-943.

Rodieck R (1988) The Primate Retina. Comparative Primate Biology 4:203-278.

Rodieck R (1998) The First Steps in Seeing. Sunderland, MA: Sinauer Associates.

Roska B, Werblin F (2001) Vertical interactions across ten parallel, stacked representations in the mammalian retina. Nature 410:583-587.

Roska B, Werblin F (2003) Rapid global shifts in natural scenes block spiking in specific ganglion cell types. Nat Neurosci 6:600-608.

Sarantis M, Mobbs P (1992) The spatial relationship between Muller cell processes and the photoreceptor output synapse. Brain Res 584:299-304.

Schnapf JL, Kraft TW, Baylor DA (1987) Spectral sensitivity of human cone photoreceptors. Nature 325:439-441.

Silveira LC, Lee BB, Yamada ES, Kremers J, Hunt DM, Martin PR, Gomes FL (1999) Ganglion cells of a short-wavelength-sensitive cone pathway in New World monkeys: morphology and physiology. Vis Neurosci 16:333-343.

Slaughter MM, Miller RF (1981) 2-amino-4-phosphonobutyric acid: a new pharmacological tool for retina research. Science 211:182-185.

Smith RG (1995) Simulation of an anatomically defined local circuit: the cone-horizontal cell network in cat retina. Vis Neurosci 12:545-561.

Smith VC, Pokorny J, Lee BB, Dacey DM (2001) Primate Horizontal Cell Dynamics: An Analysis of Sensitivity Regulation in the Outer Retina. J Neurophysiol 85:545-558.

Solomon SG, Lee BB, Sun H (2006) Suppressive Surrounds and Contrast Gain in Magnocellular-Pathway Retinal Ganglion Cells of Macaque. J Neurosci %R 101523/JNEUROSCI0821-062006 26:8715-8726.

Stafford DK, Dacey DM (1997) Physiology of the A1 amacrine: a spiking, axon-bearing interneuron of the macaque monkey retina. Vis Neurosci 14:507-522.

Sterling P (1999) Deciphering the retina's wiring diagram. Nat Neurosci 2:851.

Sterling P (2004) How retinal circuits optimize the transfer of visual information.

Stone S, Witkovsky P (1987) Center-surround organization of Xenopus horizontal cells and its modification by gamma-aminobutyric acid and strontium. Exp Biol 47:1-12.

Sun H, Smithson HE, Zaidi Q, Lee BB (2006) Specificity of Cone Inputs to Macaque Retinal Ganglion Cells. J Neurophysiol %R 101152/jn007142005 95:837-849.

Taylor WR (1996) Response properties of long-range axon-bearing amacrine cells in the dark-adapted rabbit retina. Vis Neurosci 13:599-604.

Taylor WR (1999) TTX attenuates surround inhibition in rabbit retinal ganglion cells. Vis Neurosci 16:285-290.

van Hateren H (2005) A cellular and molecular model of response kinetics and adaptation in primate cones and horizontal cells. Journal of Vision 5:331-347.

Vaney DI, Taylor WR (2002) Direction selectivity in the retina. Curr Opin Neurobiol 12:405-410.

Vardi N, Kaufman DL, Sterling P (1994) Horizontal cells in cat and monkey retina express different isoforms of glutamic acid decarboxylase. Vis Neurosci 11:135-142.

Vardi N, Duvoisin R, Wu G, Sterling P (2000) Localization of mGluR6 to dendrites of ON bipolar cells in primate retina. J Comp Neurol 423:402-412.

Verweij J, Kamermans M, Spekreijse H (1996) Horizontal cells feed back to cones by shifting the cone calcium-current activation range. Vision Research 36:3943.

Verweij J, Hornstein EP, Schnapf JL (2003) Surround antagonism in macaque cone photoreceptors. J Neurosci 23:10249-10257.

Verweij J, Kamermans M, Negishi K, Spekreijse H (1998) GABA sensitivity of spectrally classified horizontal cells in goldfish retina. Vis Neurosci 15:77-86.

Vessey JP, Lalonde MR, Mizan HA, Welch NC, Kelly MEM, Barnes S (2004) Carbenoxolone Inhibition of Voltage-Gated Ca Channels and Synaptic Transmission in the Retina. J Neurophysiol 92:1252-1256.

Vessey JP, Stratis AK, Daniels BA, Da Silva N, Jonz MG, Lalonde MR, Baldridge WH, Barnes S (2005a) Proton-mediated feedback inhibition of presynaptic calcium channels at the cone photoreceptor synapse. J Neurosci 25:4108-4117.

Vessey JP, Stratis AK, Daniels BA, Da Silva N, Jonz MG, Lalonde MR, Baldridge WH, Barnes S (2005b) Proton-Mediated Feedback Inhibition of Presynaptic Calcium Channels at the Cone Photoreceptor Synapse. J Neurosci %R 101523/JNEUROSCI5253-042005 25:4108-4117.

Vigh J, Witkovsky P (1999) Sub-millimolar cobalt selectively inhibits the receptive field surround of retinal neurons. Vis Neurosci 16:159-168.

Voipio J (1998) Diffusion and Buffering Aspects of H+, HCO3-, and CO2 Movements in Brain Tissue. In: pH and brain function. (Kaila K, Ranson BR, eds), pp 11-20. New York: John Wiley & Sons.

Volgyi B, Xin D, Amarillo Y, Bloomfield SA (2001) Morphology and physiology of the polyaxonal amacrine cells in the rabbit retina. J Comp Neurol 440:109-125.

Wassle H (2004) Parallel processing in the mammalian retina. Nat Rev Neurosci 5:747-757.

Wassle H, Boycott BB (1991) Functional architecture of the mammalian retina. Physiol Rev 71:447-480.

Werblin FS (1972) Lateral interactions at inner plexiform layer of vertebrate retina: antagonistic responses to change. Science 175:1008-1010.

Wiesel TN, Hubel DH (1966) Spatial and chromatic interactions in the lateral geniculate body of the rhesus monkey. J Neurophysiol 29:1115-1156.

Witkovsky P (2004) Dopamine and retinal function. Doc Ophthalmol 108:17-40.

Wright LL, Vaney DI (2004) The type 1 polyaxonal amacrine cells of the rabbit retina: a tracer-coupling study. Vis Neurosci 21:145-155.

Wu SM (1992) Feedback connections and operation of the outer plexiform layer of the retina. Current Opinion in Neurobiology 2:462.

Yamamoto F, Borgula GA, Steinberg RH (1992) Effects of light and darkness on pH outside rod photoreceptors in the cat retina. Exp Eye Res 54:685-697.

Yazulla S, Brecha N (1980) Binding and uptake of the GABA analogue, 3H-muscimol, in the retinas of goldfish and chicken. Invest Ophthalmol Vis Sci 19:1415-1426.

Yazulla S, Studholme KM, Vitorica J, de Blas AL (1989) Immunocytochemical localization of GABAA receptors in goldfish and chicken retinas. J Comp Neurol 280:15-26.

Zhang C-L, Wilson JA, Williams J, Chiu SY (2006) Action Potentials Induce Uniform Calcium Influx in Mammalian Myelinated Optic Nerves. J Neurophysiol %R 101152/jn000832006 96:695-709.

CURRICULUM VITAE

Christopher M. Davenport

Education

BA in Neuroscience, Johns Hopkins University, 2000
PhD in Neurobiology, University of Washington, in progress

Awards/Grants

NIH Institutional Neurobiology Training Grant 2003-2006
ARVO Retina Research Foundation Travel Grant 2006

Publications

Riccio A, Ahn S, Davenport CM, Blendy JA, Ginty DD. Mediation by a CREB family transcription factor of NGF-dependent survival of sympathetic neurons. Science 286:2358-2361. 1999.

Shcherbatko AD, Davenport CM, Speh JC, Levinson SR, Mandel G, Brehm P. Progesterone treatment abolishes exogenously expressed ionic currents in Xenopus oocytes. Am J Physiol Cell Physiol 280:C677-688. 2001.

Pocock JM, Liddle AC, Hooper C, Taylor DL, Davenport CM, Morgan SC. Activated microglia in Alzheimer's disease and stroke. Ernst Schering Res Found Workshop, 105-132. 2002.

Davenport C, Margolis D, Powers RK, Detwiler PB, Binder MD. Multiphoton fluorescence imaging of calcium fluxes in the dendrites of rat hypoglossal motoneurons. Program No. 499.6. Society for Neuroscience, 2003.

Davenport C, Packer OS, Detwiler PB, Dacey DM. Calcium imaging in primate A1 amacrine cell processes reveals evidence for functional polarity of dendritic and axon-like components. ARVO Abstracts. 2006.

Davenport CM, Detwiler PB, Dacey DM. Functional polarity of dendrites and axons of primate A1 amacrine cells. Visual Neuroscience. In Press.